A Fine Resolution HYbrid Coordinate Ocean Model (HYCOM) for the Black Sea with a New Solar Radiation Penetration Scheme: The Impact of Subsurface Heating and Attenuation Depths on the Surface Circulation

A. Birol Kara, Alan J. Wallcraft and Harley E. Hurlburt

Naval Research Laboratory, Stennis Space Center, Mississippi

(submitted to *J. Phys. Oceanogr.* on July 31, 2003)

Corresponding author address: Birol Kara: Naval Research Laboratory, Code 7323, Bldg. 1009, Stennis Space Center, MS 39529–5004, USA.

E–mail: kara@nrlssc.navy.mil, wallcraft@nrlssc.navy.mil, and hurlburt@nrlssc.navy.mil

ABSTRACT

A $1/25^\circ \times 1/25^\circ$ cos(lat), (longitude $\times$ latitude) resolution (≈ 3.2 km) eddy–resolving HYbrid Coordinate Ocean Model (HYCOM) is introduced for the Black Sea and used to examine the effects of ocean turbidity on upper ocean circulation features including sea surface height (SSH) and mixed layer depth (MLD) on annual mean climatological time scales. HYCOM is a primitive equation model with a K–Profile Parameterization (KPP) mixed layer sub–model. It uses a hybrid vertical coordinate that combines the advantages of isopycnal, sigma and z–level coordinates in optimally simulating coastal and open–ocean circulation features. This model approach with the fine resolution is applied to the Black Sea for the first time in the literature. The model uses a newly–developed time–varying solar penetration scheme that treats attenutation as a continuous quantity. This scheme involves two bands for the top 10 m of the water column; thus, it is suitable for any Ocean General Circulation Model (OGCM) that has fine vertical layer resolution near the surface. With this scheme, the depth–dependent attenuation of subsurface heating in HYCOM is given by monthly–mean fields for the attenuation of Photosynthetically Available Radiation ($k_{\rm PAR}$) during 1997–2001. These satellite–based climatological $k_{\rm PAR}$ fields are derived from Sea-viewing Wide Field-of-view Sensor (SeaWiFS) data on the spectral diffuse attenuation coefficient at 490 nm (k_{490}), and have been processed to have the smoothly–varying and continuous coverage necessary for use in the Black Sea model applications. Climatologically–forced HYCOM simulations with no assimilation of any data are then used to show the importance of including spatial and temporal varying attenuation depths for the annual mean predictions of upper ocean quantities in the Black

Sea. Results are reported from three model experiments using different values for the k_{PAR}. It is shown that a constant attenuation depth of ≈ 17 m (clear water assumption), as opposed to using spatial and temporal varying attenuation depths, changes the surface circulation, especially in the eastern Black Sea. An unrealistic subsurface warming in the former results in a weakening of the mixed layer stratification and a deep MLD. As a result, the deep MLD off Sinop (at around 35.5°E, 42.5°N) weakens the surface currents regardless of the atmospheric forcing used in the model simulations. When comparing the simulations obtained from spatial and temporal varying attenuation depths to the ones obtained from the assumption of all solar radiation at the surface case, the conclusion is that the variation of subsurface heating is less sensitive to the inclusion of realistic attenuation depths on annual time scales, because the shallow thermocline restricts the MLD in the Black Sea.

1. Introduction

The Black Sea is a nearly enclosed region connected to the Sea of Marmara and the Sea of Azov by the narrow Bosporus and Kerch Straits, respectively (Figure 1). The importance of the Black Sea extends far beyond its role as an enclosed sea because it constitutes a unique marine environment with a nearly land–locked shape, and the ventilation of the deep waters is therefore minimal. In addition, the region presents challenging test areas to study oceanographic phenomena which are dominated by coastline orientation, coastline shape and topography so it is an attractive test domain for ocean modeling studies. The Black Sea also serves as a small scale laboratory for investigation of a series of oceanographic phenomena that are common to different areas of the world ocean. Thus, it is a useful test region in developing a global ocean model.

The most important current feature in the Black Sea is a cyclonic Rim Current located along upper

continental slope (e.g., Sur et al. 1996; Oguz and Besiktepe 1999; Afanasyev et al. 2002). The Rim Current usually follows the topography of the shelf break, and it is accompanied by a series of anticyclonic mesoscale eddies as well as transient waves with an embedded train of mesoscale eddies propagating cyclonically around the basin. Previous observational studies (e.g., Oguz et al. 1993; Afanesyav et al. 2002) and fine resolution eddy–resolving Ocean General Circulation Model (OGCM) studies (e.g., Stanev and Beckers 1999; Stanev and Staneva 2000; Kourafalou and Stanev 2001; Staneva et al. 2001) examined upper ocean quantities, mainly the Rim Current, using different approaches. None of these OGCM studies, which used either Princeton Ocean Model (POM) or Modular Ocean Model (MOM), directly indicated what turbidity field they used in the mixed layer or how they treated the solar radiation attenuation in the model simulations. Thus, the missing part of the Black Sea OGCM studies is an examination of upper ocean features with respect to solar radiation penetrating into and below the mixed layer. Such an examination is necessary for the Black Sea because the sharp density stratification near the surface inhibits the ventilation of sub–pycnocline waters of the Black Sea so the euphotic structure is usually confined to the mixed layer which is directly affected by the air–sea interaction processes. Since the region is biologically active (e.g., Kideys et al. 2000; Oguz et al. 2002), it necessary for an OGCM to take water turbidity into account even if it is not coupled with a biological model. For example, variations in the attenuation of light–absorbing pigment change the vertical distribution of heating in the mixed layer, thereby affecting upper ocean dynamics.

With the availability of a remotely sensed diffuse attenuation coefficient at 490 nm (k_{490}) data set (McClain et al. 1998), it is now possible to determine the ocean turbidity at high spatial resolution and use it as part of the heat flux forcing in an OGCM in the Black Sea. By using such a data set, the time–varying

solar penetration schemes (e.g., Morel and Antonie 1994; Murtugudde et al. 2002; Morel and Maritorena 2001) can treat attenuation as a continuous quantity, which is an improvement over the use of a few discrete attenuation values corresponding to classical Jerlov water types (Jerlov 1976). However, matching attenuation of Photosynthetically Available Radiation ($k_{\rm PAR}$) to Jerlov water is needed because the original single decay formulation (e.g., $Q_{\rm sol}(z)/Q_{\rm sol}(0) = 0.49\ \exp(-z\,k_{\rm PAR})$) as used in OGCMs (e.g., Murtugudde et al. 2002; Kara et al. 2003a) is only accurate for depths deeper than 10 or 20 m. Unlike ocean models, with a bulk mixed layer, which have levels of order 10 m from the surface (e.g., Schneider and Zhu 1998; Wallcraft et al. 2003), OGCMs which have many vertical levels near the surface (e.g., Murtugudde et al. 2002; Bleck et al. 2002) often have mixed layer depths (MLDs) much shallower than 10 m and also need to distribute solar radiation within the mixed layer. Thus, a modified version of the single decay formulation is required. In this paper, we present a solar subsurface heating formulation that still treats attenutation as a continuous quantity (depending only on depth and $k_{\rm PAR}$), but is more accurate (i.e., closer to Jerlov curves from the surface downward for representative $k_{\rm PAR}$ values) in the 0–20 m range.

The main focus of this study is to set up an ocean model with hybrid coordinates for the Black Sea, using the newly–developed solar radiation penetration scheme. We then examine effects of subsurface heating on circulation dynamics of the region, including its coastal and shelf regions and the interactions of these regions with the interior of the basin and air–sea interactions. The model is applicable to the studies concerned with coastal and interior locations of the Black Sea because the hybrid coordinate is one that is isopycnal in the open, stratified ocean, but makes a dynamically smooth transition to a terrain–following coordinate in shallow coastal regions, and to z–level coordinates in the mixed layer and/or unstratified seas.

This paper is organized as follows: In section 2, spatial and temporal characteristics of attenuation depths from the remotely–sensed data in the Black Sea are introduced, as well as a new formulation representing attenuation of solar radiation with depth. In section 3, basic features of HYCOM are given. In section 4, set up of the Black Sea model is explained along with the atmospheric forcing used in the model. In section 5, the effects of ocean turbidity on the model simulations are discussed. Finally, the summary and conclusions are presented in section 6.

2. Solar Radiation Penetration

Ocean solar radiation has a strong spectral dependence with the red and near–infrared radiation absorbed within ≈ 1 m of the surface and shorter wavelengths absorbed at greater depths (e.g., Lalli and Parsons 1997). In general, the solar irradiance at the ocean surface ranges in wavelength from about 300 to 2800 nm, and is composed of three general regions: the ultra–violet (UV) below 400 nm, the visible 400–700 nm, and the infrared (IR) above 700 nm. Approximately half of the solar irradiance occurs in the infrared, and most of this is absorbed and converted to heat near the ocean surface. The remaining incident solar irradiance that penetrates to depths greater than 1 m is predominantly in the visible and UV, and this is regulated through optical absorption by the water, phytoplankton, and suspended particles. This latter portion of the spectrum is referred to as Photosynthetically Available Radiation (PAR) because it is the light available for photosynthesis by phytoplankton (e.g., Liu et al. 1994). PAR is defined as the 350–700 nm range of the spectrum, and accounts for 43–50% of the solar irradiance at the sea surface (Rochford et al. 2001). The vertical PAR distribution is a direct response to the intensity of incident solar irradiance flux entering at the sea surface (e.g., Austin and Petzold 1986) and its attenuation with depth (k_{PAR}).

As the light passes through water, it is both scattered and absorbed with different wavelengths of the visible spectrum penetrating to different depths. The influence of solar radiation differs depending on water type (Simonot and Le Treut 1986) because attenuation depth in the ocean is quite variable over the global ocean (e.g., Kara et al. 2003a). While fully spectral representations are available (Morel and Antonie 1994; Morel and Maritorena 2001), most models use simple solar irradiance approximations, such as single or bi–modal exponential parameterizations (Paulson and Simpson 1977; Zaneveld and Spinrad 1980; Simpson and Dickey 1981). The reason is that, for depths greater than 10 m, the penetrative solar flux can be accurately determined by resolving just the 300 nm to 745 nm spectral region, which is well represented by a single exponential. By using this approach, OGCM studies (Schneider and Zhu 1998; Murtugudde et al. 2002; Kara et al. 2003b) only considered solar radiation that escapes the top layer or level of the model for climate simulations. In these cases, the red and near–infrared radiation is completely absorbed within the surface layer (e.g., minimum MLD of 10 m).

2a. A New Subsurface Heating Parameterization for OGCMs

An OGCM with high vertical resolution needs at least two bands for the top 10 m of the water column. Traditional two–band Jerlov schemes differ significantly from single–band k_{PAR} between about 3 m and 15 m, with k_{PAR} less intensified than Jerlov near the surface (Figure 2). This is primarily due to the split Jerlov between "red" (near surface) and "blue" (deep) light, with k_{PAR} assuming that the 51% non–visible (primarily IR) light is absorbed at the surface and treats the remaining 49% (i.e., PAR) as one band which is biased towards blue. On the other hand, classical Jerlov types include both visible and IR light in its near surface red band and therefore has much less blue light with the amount of blue light dependent on the turbidity. For

example, the percentage of light left at about 2 m depth for Jerlov I, IA, IB, II and III types is 42%, 38%, 33%, 23% and 22% (all primarily in the blue spectrum), respectively (Table 1).

We want to modify single exponential formulation, $Q_{\rm sol}(z)/Q_{\rm sol}(0) = 0.49\,\exp(-z\,k_{\rm PAR})$ so we start with Jerlov water types at 2 m to find a new solar radiation penetration formulation for use in OGCMs. It is assumed that these numbers are appropriate for $k_{\rm PAR}$ = 1/23,1/20,1/17,1/14 because these are the blue extinction coefficients from existing schemes (Kara et al. this issue). The fit is then to determine a ratio, $\gamma = Q_{\rm blue}(0)/Q_{\rm sol}(0)$ such that

$$Q_{\rm sol}(2)/Q_{\rm sol}(0) = (1-\gamma)\exp(-2/0.5) + \gamma\exp(-2k_{\rm PAR}) \tag{1}$$

matches the Jerlov table. Note that $\exp(-2/0.5)$ is 0.0183 (1.83%) so this must be allowed for in the fit. We found that $\gamma = \max(0.27, 0.695 - 5.7k_{\rm PAR})$ by assuming that I, IA, IB is more important than II (Figure 3). Thus, the HYCOM solar subsurface heating formulations are expressed as follows:

$$Q_{\rm sol}(z)/Q_{\rm sol}(0) = (1-\gamma)\exp(-z/0.5) + \gamma\exp(-zk_{\rm PAR}), \tag{2}$$

$$\gamma = \max(0.27, 0.695 - 5.7k_{\rm PAR}). \tag{3}$$

This approach comes from matching $k_{\rm PAR}$ to the traditional Jerlov scale for the fraction in each band. The percentage of shortwave radiation under $k_{\rm PAR}$ extinction calculated from this approach is provided in Table 2.

In our formulation (Eq. 2), the red penetration scale is 2 (i.e., e–folding depth of 0.5 m), the blue penetration scale is $k_{\rm PAR}$, and a linear formula for the fraction of solar radiation in the blue band is used. The deep extinction rate is given by $\gamma\exp(-zk_{\rm PAR})$, with γ between 0.495 and 0.155, and with a typical range of 0.46 to 0.21. The new generalized HYCOM $k_{\rm PAR}$ values are shown in Figure 2 for comparisons with the

traditional Jerlov waters and the $k_{\rm PAR}$ approach based on a single band as used in Naval Research Laboratory Layered Ocean Model (NLOM) with an embedded mixed layer in predicting upper ocean quantities over the global ocean (Wallcraft et al. 2003; Kara et al. 2003b).

It should be noted that although Lewis et al. (1990) and Siegel et al. (1995) indicated solar transmission at around 20 m depth can exceed 40 W m^{-2} for a surface irradiance of 200 W m^{-2}, we find that this is possible only if $k_{\rm PAR}$=0.04, and if $k_{\rm PAR}$=0.2, 200 W m^{-2} becomes 1 W m^{-2} at 20 m (see Table 2). Earlier studies (e.g., Ohlman et al. 1998) indicated that solar radiation in the visible band within the mixed layer below 10 m can be represented with a single exponential profile to within 10% accuracy. We show that if 73% of the solar radiation is in the red exponential band, then as little as 4% of the total is left at 10 m.

The new parameterization presented here (i.e., $k_{\rm PAR}$ based Jerlov–like 2–band scheme) is somewhat consistent with the one presented by Morel and Antonie (1994) but computationally less expensive for global applications. Morel and Antonie (1994) use a 3–band scheme (IR, red and blue) with PAR that includes both red and blue bands; while, the red band in our parameterization consists of IR and red bands (i.e., non PAR plus part of PAR).

2b. Attenuation Depths in the Black Sea

Our interest is in the amount of shortwave radiation that penetrates through the mixed layer. Thus, we first show spatial variations in the annual mean shortwave radiation over the sea surface (Figure 4a,b) that was obtained from two different sources: (1) European Centre for Medium–Range Weather Forecasts (ECMWF) Re–Analysis (ERA) product (ECMWF 1995; Gibson et al. 1997), and (2) Fleet Numerical Meteorology and Oceanography Center (FNMOC) Navy Operational Global Atmospheric Prediction System (NOGAPS) data

(Rosmond et al. 2002). An annual mean was formed during 1979–1993 for ECMWF and 1998–2002 for NOGAPS. Later, we will use ECMWF and FNMOC output to investigate model sensitivity to the choice of atmospheric forcing product. While spatial distributions of shortwave radiation are different between ECMWF and NOGAPS, they usually have large values in the interior in comparison to coastal regions. The basin averaged annual mean shortwave radiation values are 135 and 163 W m^{-2} for ECMWF and NOGAPS, respectively. The amount of shortwave radiation that enters the mixed layer depends on the attenuation depths as mentioned in section 2a.

The OGCM that will be used in this paper (see section 3) takes solar radiation penetration into account through climatological monthly mean attenuations depths, so that the suburface heating can be prescribed in the model. For this purpose the monthly mean attenuation depths were obtained using a remotely sensed k_{490} data set (McClain et al. 1998) which were acquired from the Sea–viewing Wide Field–of–view Sensor (SeaWiFS) Project during the 1997–2001 observation period. SeaWiFS ocean color data provides information on radiances emitted from the sea surface at selected wavelengths. From this information the wavelength dependence of the diffuse attenuation coefficient can be constructed using the PAR portion of the solar spectrum. The SeaWiFS monthly–mean k_{490} data sets have a horizontal resolution of 9 km ($\approx 1/12^{\circ}$). Using these monthly k_{490} data sets, we construct the monthly $k_{\rm PAR}$ using the Zaneveld et al. (1993) regression relations. It is noted that even though many scenes are used to construct the monthly means, the k_{490} data still has data voids due to cloud coverage and infrequent sampling by satellite sensors, as well as incorrect and biased observations (noise). Thus, we applied a statistical interpolation method (Daley 1991) to fill in data voids during the 1997–2001 period. The monthly mean $k_{\rm PAR}$ fields were then computed from the k_{490} data and spatially interpolated

to the HYCOM domain. We will use these climatological monthly mean $k_{\rm PAR}$ fields, constrcuted during the 4–year period (1997–2001), for prescribing the subsurface heating in HYCOM simulations.

For simplicity the annual mean of the $k_{\rm PAR}$ processed from the SeaWifS data is shown in Figure 4c. The large $k_{\rm PAR}$ values are a typical feature of the attenuation coefficient in the Black Sea. The decreased transparency over the most of the Black Sea is due to the greater biological productivity that occurs from increased availability of nutrients upwelled into the euphotic zone (e.g., Kideys et al. 2000; Konovalov and Murray 2001). For the present application, the greatest interest is in those situations where subsurface heating can occur below the mixed layer. Small attenuation depth ($1/k_{\rm PAR}$) might produce complete (or almost complete) absorption of the solar radiation at the sea surface. In the western part, $k_{\rm PAR}$ values are usually greater than 0.25 $\rm m^{-1}$ which corresponds to an attenuation depth of 4 m. This implies that a turbidity increase in the region causes increased heating within the MLD because the climatological MLD is relatively shallow (Figure 4d). Note that the MLD is calculated from monthly mean temperature and salinity profiles obtained from the new 1/4° Generalized Digital Environmental Model (GDEM) climatology (NAVOCEANO, personal communication) that includes 78 levels in vertical. A variable density (σ_t) criterion with ΔT=0.5°C is used to obtain MLD (see Kara et al. (2000) for a more detailed definition of MLD).

3. HYCOM Description

HYCOM is a generalized (hybrid isopycnal/terrain–following (σ)/z–level) coordinate primitive equation model as described in Bleck (2002), in detail. The hybrid coordinate extends the geographic range of applicability of traditional isopycnic coordinate circulation models (e.g., Bleck et al. 1992) toward shallow coastal seas and unstratified parts of the ocean. Typically, HYCOM behaves like σ–coordinate model in shallow,

unstratified coastal regions, like a z–level coordinate model in the mixed layer and other unstratified regions, and like an isopycnic–coordinate model where the ocean is stratified. The model makes a dynamically smooth transition between the coordinate type via the layered continuity equation. The choice of coordinate type varies in time and space, and the optimal choice is updated every time step.

HYCOM contains a total of five prognostic equations: two momentum equations for the horizontal velocity components, a mass continuity or layer thickness tendency equation and two conservation equations for a pair of thermodynamic variables, such as salt and temperature or salt and density. The model equations, written in (x, y, s) coordinates, where s is an unspecified vertical coordinate, are

$$\frac{\partial \mathbf{v}}{\partial t_s} + \nabla_s \frac{\mathbf{v}^2}{2} + (\zeta + f)\mathbf{k} \times \mathbf{v} + \left(\frac{\partial s}{\partial t}\frac{\partial p}{\partial s}\right)\frac{\partial \mathbf{v}}{\partial p} + \nabla_s M - p\nabla_s \alpha = -g\frac{\partial \tau}{\partial p} + \left(\frac{\partial p}{\partial s}\right)^{-1} \nabla_s \cdot \left(\nu \frac{\partial p}{\partial s}\nabla_s \mathbf{v}\right), \quad (4)$$

$$\frac{\partial}{\partial t_s}\left(\frac{\partial p}{\partial s}\right) + \nabla_s \cdot \left(\mathbf{v}\frac{\partial p}{\partial s}\right) + \frac{\partial}{\partial s}\left(\frac{\partial s}{\partial t}\frac{\partial p}{\partial s}\right) = 0, \quad (5)$$

$$\frac{\partial}{\partial t_s}\left(\frac{\partial p}{\partial s}\theta\right) + \nabla_s \cdot \left(\mathbf{v}\frac{\partial p}{\partial s}\theta\right) + \frac{\partial}{\partial s}\left(\frac{\partial s}{\partial t}\frac{\partial p}{\partial s}\theta\right) = \nabla_s \cdot \left(\nu \frac{\partial p}{\partial s}\nabla_s \theta\right) + \hbar_\theta, \quad (6)$$

where $\mathbf{v} = (u, v)$ is the horizontal velocity vector, p is pressure, θ represents any one of the model's thermodynamic variables, $\alpha = 1/\rho$ is the potential specific volume, $\zeta = \partial v/\partial x_s - \partial u/\partial y_s$ is the relative vorticity, $M = gz + p\alpha$ is the Montgomery potential, $gz = \phi$ is the geopotential, f is the Coriolis parameter, $\mathbf{k}$ is the vertical unit vector, ν is a variable eddy viscosity/diffusivity coefficient, and τ is the wind– and/or bottom–drag induced shear stress vector. The variable $\hbar_\theta$ represents the sum of diabatic source terms, including diapycnal mixing acting on θ. Subscripts show which variable is held constant during partial differentiation. Distances in x, y direction, as well as their time derivatives u and v, respectively, are measured in the projection onto a horizontal plane.

The prognostic equations in the model are time–integrated using the split–explicit treatment of barotropic

and baroclinic modes (Bleck and Smith 1990). The split–explicit approach has proven to be advantageous for executing ocean models on massively parallel computers because it does not require solution of an elliptic equation. Isopycnal diffusivity and viscosity values, including the one used for thickness diffusion (interface smoothing), are formulated as $u_d \Delta x$ where Δx is the local horizontal mesh size and u_d is of order 0.01 m s^{-1}. In regions of large shear, isopycnic viscosity is set proportional to the product of mesh–size squared and total deformation (Smagorinsky 1963), the proportionality factor being 0.2.

HYCOM uses KPP mixed layer model, which is particularly attractive for several reasons. It contains improved parameterizations of physical processes in the mixed layer, including non–local effects. It has also been designed to run with relatively low vertical resolution, an advantage for OGCMs. The KPP model calculates the mixing profile from the surface to the bottom of the water column, and thus provides an estimate of diapycnal mixing beneath the mixed layer. It provides mixing throughout the water column with an abrupt but smooth transition between the vigorous mixing within the surface boundary layer and the relatively weak diapycnal mixing in the ocean interior. In the ocean interior, the contribution of background internal wave breaking, shear instability mixing, and double diffusion (both salt fingering and diffusive instability) are parameterized in the KPP model. In the surface boundary layer, the influences of wind-driven mixing, surface buoyancy fluxes, and convective instability are parameterized. The KPP algorithm also parameterizes the influence of nonlocal mixing of temperature and salinity, which permits the development of countergradient fluxes.

The main quantities used throughout this paper are sea surface height (SSH) and MLD. The SSH is a diagnostic quantity, which is sum of the Montgomery potential and barotropic pressure. The MLD is a

diagnostic quantity which depends on a specified density difference with respect to the surface. In general, the MLD is the first depth at which the density jump with respect to the surface is the equivalent of 0.2°C. By converting to density we can allow for salinity driven mixed layers. The conversion is done at the surface (i.e., with respect to sea surface temperature and sea surface salinity) so HYCOM converts the temperature jump to a local density jump and then finds the shallowest depth. The KPP mixed layer model is applied to every horizontal point independently. This sometimes lead to a very noisy MLD. Thus, a 9–point smoothing on the MLD fields is used throughout the analysis. This is a standard uniform grid 9–point smoother.

4. Black Sea Model

4a. Model Resolution and Constants

The Black Sea model used here has [$1/25^\circ \times 1/25^\circ$ cos(lat), longitude $\times$ latitude] resolution on Mercator grid. This mercator grid has square grid cells with a resolution of ($0.04 \times \cos(\text{lat}) \times 111.2$ km), i.e., 3.37 km at the southern and 3.05 km at the northern coast. Average grid resolution is $\approx$ 3.2 km. Longitudinal and latitudinal array sizes in the model are 360 and 206, respectively.

There are a total of 15 hybrid layers in the model, and the target density (σ_t) values corresponding to layers 1 through 15 are 6.00, 9.00, 10.00, 11.00, 12.00, 12.80, 13.55, 14.30, 15.05, 16.20, 16.80, 16.95, 17.05, 17.15 and 17.20, respectively. These were primarily based on the basin averaged climatological mean temperature and density fields (see section 4c), with each layer increasingly thick, the abyssal layer being the thickest. These target density values were found to be optimal in comparison to other layer density sets based on a series of tuning experiments. It is noted that the wide and shallow shelf area in the northwestern part is resolved by the first few model layers.

Constant parameters used in the Black Sea model are provided in Table 3. The sensitivity of the Black Sea model to the choice of KPP parameters was investigated by undertaking a tuning exercise to find an optimal set in providing a realistic sea surface temperature (SST) from realistic atmospheric forcing over as much of the Black Sea as possible. This was done by comparing the monthly satellite–based SST climatology to monthly averages from the model, which is similar to a statistical tuning methodology, such as introduced in Wallcraft et al. (2003). Overall, the original KPP constants reported in Large et al. (1994) worked best in the Black Sea model although we also confirmed that new KPP constants (e.g., KPP value for turbulent shear contribution to bulk Ri number and KPP value for calculating shear instability) suggested in Smyth et al. (2002) did not cause any significant changes in the model simulations.

4b. Bottom topography

Most previous Black Sea model studies used UNESCO bathymetric maps to represent bottom topography (e.g., Stanev and Stenava 2001; Stanev and Staneva 2000), and a few studies used the Earth Topography Five Minute Grid (ETOP05) data (e.g., Staneva et al. 2001). While ETOP05 (NOAA 1988) is usually adequate for deeper parts of the ocean, it is less reliable over continental shelves (< 200 m deep) because of mismatches in the chart isobaths used in constructing the data set. As a result, it poses a problem for the Black Sea because of the existence of the wide continental shelf.

The bottom topography in the Black Sea model (Figure 5) was constructed from Digital Bathymetric Data Base–Variable resolution (DBDB–V) data set developed by Naval Oceanographic Office (NAVOCEANO). The DBDB–1.0 (NAVOCEANO 1997; 2001) used in HYCOM has a resolution of $1'$ (1 minute). After interpolation to the Black Sea model grid, the final topography was also smoothed twice with a 9–point smoother

to reduce energy generation at small scales. In general, the Black Sea has an almost flat abyssal plain, a flat wide shelf in the northwestern part and a steep continental slope along the Turkish coast (see Figure 5).

4c. Temperature and Salinity Initialization

Previous modeling studies of the Black Sea were limited to use of local data sets constructed from sparse observations for the initial temperature and salinity climatology (e.g., Altman et al. 1987; Truckhchew and Demin 1992). There is also uncertainity in the quality of these existing data sources in the Black Sea (e.g., Staneva and Stanev 1998). A well–documented commonly used subsurface temperature and salinity climatology from the $1^\circ \times 1^\circ$ World Ocean Atlas 1994 (Levitus et al. 1994; Levitus and Boyer 1994) does not cover the Black Sea region. While a recently updated World Ocean Atlas (Conkright et al. 2002) includes monthly mean temperature and salinity climatologies, it is still at $1^\circ \times 1^\circ$ grid resolution, which does not resolve the coastal and shelf regions. Thus, the Black Sea suffers from lack of quality fine resolution subsurface temperature and salinity climatologies which can be used for model initialization.

In this paper, HYCOM is initialized using the temperature and salinity from the Modular Ocean Data Assimilation System (MODAS) climatology developed at NRL (Fox et al. 2002) because it provides increased horizontal resolution. The climatology has variable grid resolution: $1/8^\circ$ near land, $1/4^\circ$ over shallow shelves, and $1/2^\circ$ in the open ocean. This makes the MODAS climatology a candidate to use in studying the surface circulation. In general, the MODAS climatology is one of the current Navy standard tools for production of three dimensional grids of temperature and salinity, and derived quantities such as density (Harding et al. 1999). The MODAS includes both a static climatology and a dynamic climatology. The former that represents the historical averages is used here. Climatological potential temperature, salinity and density

fields from MODAS are output at 27 depth levels ranging from 0 to 2200 m for the Black Sea (Figure 6).

In general, the Black Sea can be described as a two–layer system with a thin low salinity surface layer overlying a relatively uniform higher salinity deep layer (see Figure 6). Murray et al. (1991) and Ozsoy et al. (1993) showed that the Cold Intermediate Layer (CIL) is characterized by temperatures less than 8°C, which occurs within a typical range of about 50 to 180 m overlying the main pycnocline where vertical stratification is maintained by the salinity gradient. This layer is located under the summer thermocline and above the halocline. Salinity increases from 17.8 psu at the sea surface to 23.0 psu at 500 m.

4d. Wind and Thermal Forcing

HYCOM reads in the following time–varying atmospheric forcing fields: wind stress and thermal forcing (air temperature and air mixing ratio at 10 m above the sea surface, net shortwave radiation and net longwave radiation at the sea surface). For the Black Sea model we constructed wind/thermal forcing from two different archived operational weather center products: (1) $1.125^\circ \times 1.125^\circ$ ECMWF Re–Analysis (ERA) climatology (1979–1993), and (2) $1^\circ \times 1^\circ$ NOGAPS climatology (1998–2002).

All model simulations are performed using climatological monthly mean forcing fields. However, a high frequency component is added to the climatological forcing because the mixed layer is sensitive to variations in surface forcings on time scales of a day or less (e.g., Wallcraft et al. 2003; Kara et al. 2003b) and because the future goal is to perform simulations forced by high frequency interannual atmospheric fields from operational weather centers. Hybrid winds consist of monthly ECMWF (or NOGAPS) plus ECMWF wind anomalies. Construction of the ECMWF hybrid winds is briefly described here. The same procedure is applied to NOGAPS. For HYCOM wind stress forcing ($\vec{\tau}_{HYCOM}$), 6–hourly intra–monthly anomalies from ECMWF

are used in combination with the monthly mean wind stress climatology of ECMWF (NOGAPS) interpolated to 6 hourly intervals. The 6 hourly anomalies are obtained from a reference year. For the purpose the winds from September 1994 through September 1995 (6–hourly) are used, inclusive, because they represented a typical annual cycle of the ECMWF winds, and because the September winds in 1994 and 1995 most closely matched each other. The 6–hourly September 1994 and September 1995 wind stresses are blended to make a complete annual cycle, which is denoted by $\vec{\tau}_{ECMWF}$. The ECMWF wind stresses are calculated from ECMWF 10 m winds using the bulk formulae of Kara et al. (2002). Monthly averages are first formed from the September 1994 through September 1995 ECMWF wind stresses ($\vec{\tau}_{ECMWF}$) to create the ECMWF wind stress anomalies ($\vec{\tau}_A$), and are then linearly interpolated to the time intervals of the 6–hourly ECMWF winds to produce a wind stress product ($\vec{\tau}_I$). The anomalies are then obtained by applying the difference ($\mathrm{A}\vec{\tau}_A = \vec{\tau}_{ECMWF} - \vec{\tau}_I$). Scalar wind speed is obtained from the input wind stress and therefore has 6–hourly variability. Note that NOGAPS provides surface stress directly so the high frequency component ($\vec{\tau}_A$) is added to the interpolated monthly mean wind stress from NOGAPS.

The net surface heat flux that has been absorbed (or lost) by the upper ocean to depth z, $Q(0)$, is parameterized as the sum of the downward surface solar irradiance (Q_{sol}), upward longwave radiation (Q_{LW}), and the downward latent and sensible heat fluxes (Q_L and Q_S, respectively).

$$Q(z) = (Q_{\mathrm{sol}}(0) - Q_{\mathrm{sol}}(z)) - Q_{\mathrm{LW}} + Q_L + Q_S, \tag{7}$$

where Q_{sol} as described section 2a. Here $Q_{\mathrm{sol}}(z)$ is the amount of solar radiation that penetrates to depth. The rate of heating/cooling of each layer is simply obtained by evaluating (7) at the bottom and top of the layer, with only $Q_{\mathrm{sol}}(z)$ non–zero below layer 1. The model reads in monthly mean k_{PAR} fields to include effects of

turbidity as explained (see section 2b).

Latent and sensible heat fluxes at the air–sea interface are calculated using efficient and computationally inexpensive bulk formulae that include the effects of dynamic stability (Kara et al. 2002). The combination of accuracy and ease of computation makes this method preferred for computing air–sea fluxes in the HYCOM. Note that both sensible and latent heat fluxes are calculated using top layer temperature at each model time step. Including air temperature and model SST in the formulations for latent and sensible heat flux automatically provides a physically realistic tendency towards the correct SST. Radiation flux (shortwave and longwave fluxes) is so dependent on cloudiness that this is taken directly from ECMWF (or NOGAPS) for use in the model.

The Black Sea model treats rivers as a "runoff" addition to the surface precipitation field. The flow is first applied to a single ocean grid point and smoothed over surrounding ocean grid points, yielding a contribution to precipitation in m s^{-1}. This works independently of any other surface salinity forcing. Looking more closely at the largest rivers in a given ocean model domain is important to represent evaporation and precipitation effects properly. However, the problem is knowing that one data source is more accurate than another. There are several readily available river discharge climatologies, and climatological annual mean river flow values constructed from these sources are given in Table 4 for each river discharged into the Black Sea (Table 5). HYCOM reads in monthly mean river discharge values. The monthly mean RivDIS climatology (Vörösmarty et al. 1997; 1998) is preferred for use in HYCOM because it gives river inflow values at the mouth of the river. A total of 6 major rivers is used as precipitation forcing. The Danube River has the largest discharge into the Black Sea with a river flow of 6365.0 m^3 s^{-1} (0.006365 Sv). In the simulations described here HYCOM

does not include the direct Bosporus inflow, causing an imbalance in evaporation minus precipitation. This imbalance in the model was handled by adding a negative river precipitation (i.e., a river evaporation) for the Bosporus.

4e. Model Simulations

Climatologically–forced model simulations that use three different sets of k_{PAR} values are performed to investigate the effects of ocean turbidity on the sea surface circulation. Table 6 gives a brief explanation of each simulation. For expt 1, spatially and monthly varying k_{PAR} values interpolated to the HYCOM grid are used. For expt 2, all solar radiation is absorbed at the sea surface by using a unrealistically large k_{PAR} value of 99.9 m^{-1}. For expt 3, the ocean turbidity over the Black Sea is set to a constant, $k_{\mathrm{PAR}} = 0.06$ m^{-1}, which is a representative value for clear water (e.g., Kara et al. 2003a). These experiments (i.e., expts 1, 2 and 3) use wind/thermal forcing from ECMWF; while, expts 4, 5 and 6 are essentially twins of expts 1, 2 and 3 but use wind/thermal forcing from NOGAPS. All of the HYCOM simulations presented in this paper were performed with no assimilation of any oceanic data except initialization from climatology and relaxation to sea surface salinity. The model was run until it reached statistical equilibrium using 6 hourly climatological forcing as described earlier. It takes about 5–8 model years for a simulation to reach equilibrium.

5. Results and Discussion

In this section, sensitivity of model results to water turbidity is examined with a particular focus on upper ocean currents and sea surface height (SSH). All model results are presented based on annual means that were constructed from the last 4 years of the model simulations. At least a 4–year mean was needed because the 3.2 km HYCOM is nondeterministic and flow instabilities are a major contribution at this resolution.

The surface circulation in the Black Sea is dominated by meanders, eddies and dipole structures (e.g., Oguz and Besiktepe 1999). This is evident from surface current and SSH snapshots from the 3.2 km HYCOM simulations (Figure 7). Given that the Rossby radius of deformation in the Black Sea is $\approx$ 20–25 km, it is clear that the radii of coastal eddies in the model range from one to a few times the radius of deformation and are especially prevalent in the eastern half of the Black Sea. This is somewhat consistent with the results reported from a $1/12^{\circ}$ ($\approx$ 9.0 km) z–level OGCM (Staneva et al. 2001) which was forced with monthly mean atmospheric parameters (Sorkina 1974; Altman and Kumish 1986).

When using different atmospheric forcing products, the location and number of eddies in the simulations are quite different in some regions, especially in the easternmost of Black Sea. In the case of ECMWF wind/thermal forcing (expt 1) there are almost no eddies present near the Sea of Azov; while, two small eddies exist in the case of NOGAPS wind/thermal forcing (expt 4). In addition to the differences in the sizes and locations of the small eddies, the SSH values for expts 1 and 4 are also different by up to $\approx$ 8 cm in some regions, especially near the northeastern coast.

The HYCOM simulations do not show significant changes in the surface circulation and SSH when all radiation is absorbed in the surface layer (expts 2 and 5) rather than using the solar radiation penetration scheme involving realistic attenuation depths (expts 1 and 4). This is because the Black Sea is very turbid. On the other hand, the clear water constant attenuation depth assumption (i.e., $k_{\rm PAR}$= 0.06 m^{-1} $\approx$ 17 m) in expts 3 and 6 shows very different surface circulation structure and SSH variability, mostly east of 39°E where attenuation coefficients (depths) are small (large) in comparison to other parts of the region (see Figure 4). This result may seem unexpected. The reason is that even though the turbidity in the eastern Black Sea is

relatively low compared to other regions of the Black Sea, it is still high compared to most of the global ocean (Kara et al. 2003a). In addition, the seasonal cycle is relatively strong in the eastern Black Sea, and it has a strong mesoscale variability component associated with it (e.g., Stanev and Staneva 2000).

Annual mean surface currents and SSH fields for expts 1 through 6 are shown in Figure 8. The clear water constant attenuation depth assumption (expts 3 and 6) results in different current structure in comparison to the standard cases (expts 1 and 4) in the eastern Black Sea. As illustrated in Figure 7, the SSH variability in the eastern gyre and off Sinop are also different. In general, as indicated in Ozsoy and Unluata (1997), the coastal eddies which have time scales of only a few days usually merge, causing the larger eddies to form on longer time scales as is evident in the HYCOM annual mean surface current fields. There is a permanent current system encircling the Black Sea basin cyclonically over the continental slope zone. It is accompanied by a series of persistent anticyclonic mesoscale eddies as well as transient waves with mesoscale eddies propagating cyclonically around the basin.

The large scale cyclonic circulation in the Black Sea is driven by the wind stress curl. This is a well–known feature of the Black Sea as previously noted in other OGCM studies (e.g., Stanev and Beckers 1999; Kourafalou and Stanev 2001). However, it is also clear that this feature is largely independent of the atmospheric forcing product choices made here. These results are not entirely consistent with previous OGCM studies. For example, Stanev and Beckers (1999) used a three–dimensional primitive equation GeoHydrodynamics Environment Research (GHER) 3D model with a resolution of 15 km $\times$ 12 km. They reported the lowest SSH values in the eastern cyclonic gyre, indicating substantial differences in the wind stress since this pattern is controlled by the wind stress curl. The 3.2 km HYCOM with a finer resolution than the GHER 3D also shows realistic lowest

values in the western cyclonic gyre for both ECMWF and NOGAPS forcing cases (expts 1 and 4, respectively).

Another interesting feature of the surface currents shown in all the HYCOM simulations is a well–defined mean eddy south of 43°N between 34°E and 36°E (Figure 8). This is known as the Sinop eddy, a feature missing from the annual mean surface current map of Stanev and Beckers (1999). In an analysis of available hydrographic data by Oguz et al. (1993), the Sinop anticyclonic eddy emerged as one of dominant features of the Black Sea circulation, a result consistent with the HYCOM simulations.

A zonal temperature cross–section analysis is performed along 42.62°N (Figure 9) to explain the differences in stratification between expts 1, 2 and 3 (also expts 4, 5 and 6). This section was chosen because it crosses major current systems including the mean eddy off Sinop (see Figures 1 and 8). The main purpose is to see how the subsurface heating affects annual mean stratification and surface circulation. Figure 9 shows dramatically the impact of turbidity on stratification, MLD and SST. Absorbing all radiation at the surface (expts 2 and 5) does not cause any significant difference in comparison to the standard cases (expts 1 and 4). This shows only a small effect from realistic mixed layer flux. The stratification is obviously deeper and weaker when using a constant attenuation coefficient value of 0.06 m^{-1} (see Figure 9c,f) as expected. This is because of increased shortwave radiation below the sea surface. For example, $\approx$ 20% is absorbed below 20 m (see Figure 2). Thus, using the constant clear water attenuation depth, rather than realistic attenuation depths from SeaWiFS, results in excessive warming below the mixed layer. For example, the depth of the 11.5°C isotherm is $\approx$ 20 m in expt 1, while it is $\approx$ 35 m in expt 3.

In general, using a constant clear water constant attenuation depth assumption in the HYCOM simulations (expts 3 and 6) results in a relatively deep MLD in comparison to the standard simulations (expts 1 and

4) which used realistic attenuation depths (Figure 10). The reason is that the warming of the water column below the mixed layer leads to a weakening of the stratification, and this facilities deepening of the mixed layer. This is particularly evident in the deep MLD and less organized stratification between 34°E and 37°E off Sinop, especially in expt 6.

Expts 1 and 2 (similarly expts 4 and 5) produce an annual mean MLD that is shallower than the annual mean compensation depth along 42.62°N, while annual mean MLD from expt 3 (similarly expt 6) is clearly deeper than the compensation depth off Sinop. Here the compensation depth $D_C = \ln(0.01)/k_{\rm PAR}$ is defined as the depth at which the PAR decreases to 1% of its surface value (e.g., Lalli and Parsons 1997). In the present context D_C represents the maximum depth for solar heating of the upper ocean. Therefore, there is little solar penetration below the mixed layer when the MLD exceeds the D_C. However, in expts 1 and 4 MLD never exceeds the maximum D_C over the annual cycle, showing net sub–mixed layer heating in the annual mean along 42.62°N latitude belt. It is also noticed that NOGAPS wind/thermal forcing(expt 4) results in stronger currents off Trabzon in comparison to the ECMWF wind/thermal forcing case (expt 1), showing effects of atmospheric forcing on the model simulations. For example, the shortwave radiation from NOGAPS is significantly larger (by $\approx$ 60 W m^{-2}) than that from ECMWF around 40–41°E, while MLDs are similar to each other. The reason is that the temperature shear across the mixed layer is almost same in both cases because of some adjustment in the total (seasonal) heat flux (not shown).

In comparison to the climatological MLD (see Figure 4d), the root–mean–square (RMS) differences are $\approx$ 5.7, 5.6 and 10.1 m for expts 1, 2 and 3, respectively. This means that using a constant attenuation depth value of 17 m in expt 3 gave an RMS increase in MLD of $\approx$ 77% (i.e., from 5.7 to 10.1 m). We find similar

RMS differences for expts 4, 5 and 6 with values of 6.3, 6.3, and 10.9 m, respectively. Thus, using a constant clear water attenuation depth value yielded unrealistically deep MLDs for both of the atmospheric forcing sets. Associated with the strong stratification near the surface (Figure 9a,d) and the variation in the MLD RMS deviation from climatology are substantial changes in the subsurface temperatures and thermal stratification (Figure 9c and f). Overall, subsurface temperatures from the standard simulations (expts 1 and 4) also agree with those from MODAS climatology.

6. Summary and Conclusions

The purpose of this research is to (1) develop a solar radiation penetration scheme for OGCMs which use attenuation depths from remotely–sensed data, (2) implement this scheme into the HYbrid Coordinate Ocean Model (HYCOM), (3) use HYCOM with this solar radiation penetration scheme to model the Black Sea at ≈ 3.2 km resolution, and (4) use model simulations to examine the impact of subsurface heating on the upper ocean circulation structure.

The model simulations do not include assimilation of any ocean data, except for initialization from climatology and relaxation to bi–monthly climatological surface salinity. The hybrid vertical coordinate in HYCOM has isopycnal coordinates in the stratified interior but makes a dynamically smooth transition to depth coordinates in the unstratified mixed layer and terrain–following (σ) coordinate in shallow water. The optimal coordinate for each grid point and each layer is chosen every time step using the layered continuity equation and a hybrid coordinate generator.

The solar radiation penetration scheme presented in this paper treats attenuation as a continous quantity and is applicable to any OGCM that has fine vertical resolution near the surface. The climatological monthly

mean k_{PAR} fields used in the parameterization of the solar radiation penetration are derived from the remotely–sensed Sea–viewing Wide Field-of-view Sensor (SeaWiFS) data during 1997–2001. These fields provide the first complete data sets of subsurface optical properties that can be used for Black Sea model applications to subsurface heating and bio–optical processes.

The HYCOM simulations show that assuming all shortwave radiation absorbed at the surface yields annual mean sea surface currents that which are similar to those simulated using spatial and temporal turbidity fields on climatological time scales. A single Jerlov class cannot be used for any model that includes both the Black Sea and any other Sea (e.g., entire Atlantic or entire global ocean). This means that a basin–scale model which would typically use clear water (Jerlov IA) will not perform well work in predicting Black Sea upper ocean quantities, such as sea surface currents and mixed layer depth (MLD). The climatological annual mean results discussed here show that any ocean model study of existing Black Sea circulation needs to use either all shortwave radiation absorbed at the surface or to use a realistic turbidity via attenuation depths from remotely–sensed data (e.g., SeaWiFS). The results also clearly suggest that if the Black Sea turbidity is entirely or largely due to biology, a lack of nutrients (or another causes for a loss of biomass) will have a significant impact on the overall Black Sea circulation. However, a specific examination of Black Sea biosystem robustness is not made here.

Results presented in this paper reveal that the direct effect of the including space/time varying attenuation depths in the Black Sea is a shallowing of the MLD. This occurs because the heat is not deposited below the MLD in contrast to the clear water constant attenuation depth simulation. The deepening of the MLD when using the clear water attenuation depth of 17 m increases the heat content of the upper ocean

and weakens the stratification at the base of the mixed layer. As a result, changes in the surface currents also occur such as a weaker mean eddy off Sinop (at around 35.5°E, 42.5°N) regardless of the atmospheric forcing product and pronounced changes in the easternmost Black Sea (e.g., off Trabzon).

This paper focusses on the sensitivity of annual mean upper ocean quantities (sea surface currents, sea surface height and MLD) to subsurface heating in the Black Sea. Kara et al. (this issue) discusses SST predictions from HYCOM in the Black Sea, including extensive model–data comparisons. Monthly analysis and interannual simulations will be addressed in other papers. Finally, it should be noted that the Black Sea model is part of an ongoing global HYCOM development effort and will be a component of the resulting global ocean prediction system, which is planned for use at the Naval Oceanographic Office, Stennis Space Center, USA, starting in 2006.

Acknowledgments

We would like to extend our special thanks to E. J. Metzger of the Naval Research Laboratory (NRL) at the Stennis Space Center for processing and providing surface forcing fields for the model runs. Numereous discussions with Rainer Bleck of the Atmospheric and Climate Science at the Center for Nonlinear Studies (CNLS) at the Los Alamos National Laboratory (LANL), Eric Chassignet and George Halliwell at the University of Miami, Rosenstiel School of Marine and Atmospheric Science (RSMAS), during HYCOM development are greatly appreciated. The ocean color data used in this paper were obtained from the Goddard Distributed Active Archive Center under the auspices of the National Aeronautics and Space Administration (NASA). This data set is used in accord with the Sea–viewing Wide Field–of–view Sensor (SeaWiFS) Research Data Use Terms and Conditions Agreement. The numerical HYCOM simulations were performed under the De-

partment of Defense High Performance Computing Modernization Program on a IBM SP POWER3 at the Naval Oceanographic Office, Stennis Space Center, Mississippi and on a HP/COMPAQ SC45 at the United States Army Engineer Research and Development Center (ERDC), Vicksburg, Mississippi. This is contribution NRL/JA/7320/03/0008 and has been approved for public release.

References

Afanasyev, Y. D., A. G. Kostianoy, A. G. Zatsepin, and P.–M. Poulain, 2002: Analysis of velocity field in the eastern Black Sea from satellite data during the Black Sea '99 experiment. *J. Geophys. Res.*, **13**, 1–8.

Altman, E. N., I. F. Gertman, and Z. A. Golubeva, 1987: Climatological fields of salinity and temperature in the Black Sea. State Oceanogr. Inst. Tech. Rep., 109 pp (in Russian). [Available from the State Oceanography Institute, Sevastopol Branch, Sevastopol, Ukraine.]

——, and N. I. Kumish, 1986: Interannual and seasonal variability of the Black Sea fresh water balance. *Trudy Gos. Oceanogr. Inst.*, **145**, 3–15 (in Russian).

Austin, R. W., and T. J. Petzold, 1986: Spectral dependence of the diffuse attenuation coefficient of light in ocean waters. *Opt. Eng.*, **25**, 471–479.

Bleck, R., 2002: An oceanic general circulation model framed in hybrid isopycnic–cartesian coordinates. *Ocean Modelling*, **4**, 55–88.

——, C. Rooth, D. Hu, and L. Smith, 1992: Salinity–driven thermocline transients in a wind– and thermohaline–forced isopycnic coordinate model of the North Atlantic. *J. Phys. Oceanogr.*, **32**, 1486–1505.

——, and L. Smith, 1990: A wind–driven isopycnic coordinate model of the north and equatorial Atlantic Ocean. 1. Model development and supporting experiments. *J. Geophys. Res.*, **95**, 3273–3285.

Conkright, M. E., R. A. Locarnini, H. E. Garcia, T. D. O'Brien, T. P. Boyer, C. Stephens, and J. I. Antonov, 2002: *World Ocean Atlas 2001: Objective Analyses, Data Statistics, and Figures, CD–ROM Documentation.* National Oceanographic Data Center, Silver Spring, MD, 17 pp.

ECMWF, 1995: User guide to ECMWF products. *Meteorol. Bull. M3.2*, 71 pp. [Available from ECMWF, Shinfield Park, Reading RG2 9AX, UK.]

Daley, R., 1991: *Atmospheric Data Analysis.* Cambridge University Press, New York, 457 pp.

Fox, D. N., W. J. Teague, C. N. Barron, M. R. Carnes, and C. M. Lee, 2002: The Modular Ocean Data Assimilation System (MODAS). *J. Atmos. Oceanic Technol.*, **19**, 240–252.

Gibson, J. K., P. Kållberg, S. Uppala, A. Hernandez, A. Nomura, and E. Serrano, 1997: ERA description. ECMWF Re–Analysis Project Report Series, No. 1, 72 pp. [Available from ECMWF, Shinfield Park, Reading RG2 9AX, UK.]

Harding, J. M., M. R. Carnes, R. H. Preller, and R. Rhodes, 1999: The Naval Research Laboratory role in naval ocean prediction. *Mar. Technol. Soc. J.*, **33**, 67–79.

Jerlov, N. G., 1976: *Marine Optics. Elseiver Ocean. Ser.*, **14**, Elseiver, New York, 231 pp.

Kara, A. B., H. E. Hurlburt, P. A. Rochford, and J. J. O'Brien, 2003a: The impact of water turbidity on the interannual sea surface temperature simulations in a layered global ocean model. *J. Phys. Oceanogr.*, in review.

——, A. J. Wallcraft, and H. E. Hurlburt, 2003b: Climatological SST and MLD simulations from NLOM with an embedded mixed layer. *J. Atmos. Oceanic Technol.*, in press.

——, P. A. Rochford, and H. E. Hurlburt, 2002: Air–sea flux estimates and the 1997–1998 ENSO event.

Bound.–Layer Meteor., **103**, 439–458.

——, ——, and ——, 2000: An optimal definition for ocean mixed layer depth. *J. Geophys. Res.*, **105**, 16 803–16 821.

Kideys, A. E., A. V. Kovalev, G. Shulman, A. Gordina, and F. Bingel, 2000: A review of zooplankton investigations of the Black Sea over the last decade. *J. Mar. Sys.*, **24**, 355–371.

Konovalov, S. K., and J. W. Murray, 2001: Variations in the chemistry of the Black Sea on a time scale of decades (1960–1995). *J. Mar. Sys.*, **31**, 217–243.

Kourafalou, V. H., and E. V. Stanev, 2001: Modeling the impact of atmospheric and terrestrial inputs on the Black Sea coastal dynamics. *Ann. Geophysicae*, **19**, 245–256.

Lalli, C. M., and T. R. Parsons, 1997: *Biological Oceanography: An Introduction.* Butterworth–Heinemann, Woburn, Mass., 314 pp.

Large, W. G., J. C. McWilliams, and S. C. Doney, 1994: Oceanic vertical mixing: A review and a model with a nonlocal boundary layer parameterization. *Rev. Geophys.*, **32**, 363–403.

Levitus, S., R. Burgett, and T. P. Boyer, 1994: *World Ocean Atlas 1994, Volume 3: Salinity.* NOAA Atlas NESDIS 3, U.S. Govt. Printing Office, Washington, D.C., 99 pp.

——, and T. P. Boyer, 1994: *World Ocean Atlas 1994, Volume 4: Temperature.* NOAA Atlas NESDIS 4, U.S. Govt. Printing Office, Washington, D.C., 117 pp.

Lewis, M. R., M. E. Carr, G. Feldman, C. R. McClain, and W. Esaias, 1990: Influence of penetrating radiation on the heat budget of the equatorial Pacific Ocean. *Nature*, **347**, 543–545.

Liu, W. T., A. Zhang, and J. K. B. Bishop, 1994: Evaporation and solar irradiance as regulators of sea surface

temperature in annual and interannual changes. *J. Geophys. Res.*, **99**, 12 623–12 637.

McClain, C. R., M. L. Cleave, G. C. Feldman, W. W. Gregg, S. B. Hooker, and N. Kuring, 1998: Science quality SeaWiFS data for global biosphere research. *Sea Tech.*, **39**, 10–16.

Morel, A., and S. Maritorena, 2001: Bio–optical properties of oceanic waters: A Reappraisal. *J. Geophys. Res.*, **106**, 7163–7180.

——, and D. Antonie, 1994: Heating rate within the upper ocean in relation to its bio–optical state. *J. Phys. Oceanogr.*, **24**, 1652–1665.

Murtugudde, R., J. Beauchamp, C. R. McClain, M. R. Lewis, and A. J. Busalacchi, 2002: Effects of penetrative radiation on the upper tropical ocean circulation. *J. Climate*, **15**, 470–486.

Murray, J. W., Z. Top, and E. Ozsoy, 1991: Hydrographic properties and ventillation of the Black Sea. *Deep Sea Res.*, **38**, 663–690.

Naval Oceanographic Office (NAVOCEANO), 2001: Naval Oceanographic Office Data Model, Hydrography/Bathymetry. [Available online at http://128.160.23.42/dbdbv/database_doc.html]

——, 1997: Database description for Digital Bathymetric Data Base–Variable Resolution (DBDB–V), version 1.0. Naval Oceanographic Office, Stennis Space Center, MS.

NOAA, 1988: Digital Relief of the Surface of the Earth. Data Announcement 88–MGG–02. [Available from NOAA National Geophysical Data Center, E/GC 325 Broadway, Boulder, Colorado 80305–3328, USA.]

Oguz, T., P. Malanotte–Rizzoli, H. W. Ducklow, and J. W. Murray, 2002: Interdisciplinary studies integrating the Black Sea biogeochemistry and circulation dynamics. *Oceanography*, **15**, 4–11.

——, and S. Besiktepe, 1999: Observations on the Rim Current structure, CIW formation and transport in

the Western Black Sea. *Deep Sea Res.* Part I, **46**, 1733–1753.

——, V. Latun, M. A. Latif, V. Vladimirov, H. I. Sur, A. Markov, E. Ozsoy, B. Kotovshchikov, V. Eremeev, and U. Unluata, 1993: Circulation in the surface and intermediate layers of the Black Sea. *Deep Sea Res.*, Part 1, **40**, 1597–1612.

Ohlmann, J. C., D. Siegel, and L. Washburn, 1998: Radiating heating of the western equatorial Pacific during TOGA–COARE. *J. Geophys. Res.*, **103**, 5379–5395.

Ozsoy, E., and U. Unluata, 1997: Oceanography of the Black Sea: A review of some recent results. *Earth Sci. Rev.*, **42**, 231–272.

——, ——, and Z. Top, 1993: The evaluation of Mediterranean water in the Black Sea: Interior mixing and material transport by double diffusive intrusions. *Prog. Oceanogr.*, **31**, 275–320.

Paulson, C. A., and J. J. Simpson, 1977: Irradiance measurements in the upper ocean. *J. Phys. Oceanogr.*, **7**, 952–956.

Perry, G. D., P. B. Duffy, and N. L. Miller, 1996: An extended data set of river discharges for validation of general circulation models. *J. Geophys. Res.*, **101**, 21 339–21 349.

Rochford, P. A., A. B. Kara, A. J. Wallcraft, and R. A. Arnone, 2001: Importance of solar subsurface heating in ocean general circulation models. *J. Geophys. Res.*, **106**, 30 923–30 938.

Rosmond, T. E., J. Teixeira, M. Peng, T. F. Hogan, and R. Pauley, 2002: Navy Operational Global Atmospheric Prediction System (NOGAPS): Forcing for ocean models. *Oceanography*, **15**, 99–108.

Schneider, E. K., and Z. Zhu, 1998: Sensitivity of the simulated annual cycle of sea surface temperature in the equatorial Pacific to sunlight penetration. *J. Climate*, **11**, 1933–1950.

Siegel, D. A., J. C. Ohlmann, L. Washburn, R. Bidigare, C. Nosse, E. Fields, and Y. Zhou, 1995: Solar radiation, phytoplankton pigments and radiant heating of the equatorial Pacific. *J. Geophys. Res.*, **100**, 4885–4891.

Simonot, J.–Y., and H. Le Treut, 1986: A climatological field of mean optical properties of the world ocean. *J. Geophys. Res.*, **91**, 6642–6646.

Simpson, J. J., and T. D. Dickey, 1981: Alternative parameterizations of downward solar irradiance and their dynamical significance. *J. Phys. Oceanogr.*, **11**, 876–882.

Smagorinsky, J. S., 1963: General circulation experiments with the primitive equations. I: The basic experiment. *Mon. Wea. Rev.*, **91**, 99–164.

Smyth, W. D., E. D. Skyllingstad, G. Crawford, and H. Wijesekera, 2002: Nonlocal fluxes and Stokes drift effects in the K–Profile Parameterization. *Ocean Dyn.*, **52**, 104–115.

Sorkina, A. I., 1974: *Reference Book on the Black Sea Climate.* Gidrometeoizdat, Moscow, 406 pp (in Russian).

Stanev, E. V., and J. V. Staneva, 2001: The sensitivity of the heat exchange at ocean surface to meso and sub–basin scale eddies. Model study for the Black Sea. *Dyn. Atmos. Oceans*, **33**, 163–189.

——, and J. V. Staneva, 2000: The impact of the baroclinic eddies and basin oscillations on the transitions between different quasi–stable states of the Black Sea circulation. *J. Mar. Sys.*, **24**, 3–26.

——, and J. M. Beckers, 1999: Barotropic and baroclinic oscillations in strongly stratified ocean basins. Numerical study for the Black Sea. *J. Mar. Sys.*, **19**, 65–112.

Staneva, J. V., D. E. Dietrich, E. V. Stanev, and M. J. Bowman, 2001: Rim Current and coastal eddy mechanisms in an eddy–resolving Black Sea general circulation. *J. Mar. Sys.*, **31**, 137–157.

——, and E. V. Stanev, 1998: Oceanic response to atmospheric forcing derived from different climatic data sets. *Ocean. Acta*, **21**, 393–417.

Sur, H. I., and Y. P. Ilyin, 1997: Evolution of satellite derived mesoscale thermal patterns in the Black Sea. *Prog. Oceanogr.*, **39**, 109–151.

Sur, H. I., E. Ozsoy, Y. P. Ilyin, and U. Unluata, 1996: Coastal/deep ocean interactions in the Black Sea and their ecological/environmental impacts. *J. Mar. Sys.*, **7**, 293–320.

Truckhchew, D. I., and Y. L. Demin, 1992: The Black Sea general circulation and climatic temperature and salinity fields. Woods Hole Oceanographic Inst. Tech. Rep., WHOI–92-34. [Available from MBL/WHOI Library, 7 MBL Street, Woods Hole, MA 02543, USA.]

Vörösmarty, C. J., K. Sharma, B. M. Fekete, A. H. Copeland, J. Holden, J. Marble, and J. A. Lough, 1997: The storage and aging of continental runoff in large reservoir systems of the world. *Ambio*, **26**, 210–219.

——, B. M. Fekete, and B. A. Tucker, 1998: Global River Discharge Database (RivDIS) V1.1. [Available from the ORNL Distributed Active Archive Center, Oak Ridge National Laboratory, Oak Ridge, TN, USA.]

Wallcraft, A. J., A. B. Kara, H. E. Hurlburt, and P. A. Rochford, 2003: The NRL Layered Global Ocean Model (NLOM) with an embedded mixed layer sub–model: Formulation and tuning. *J. Atmos. Oceanic Technol.*, submitted.

Zaneveld, J. R. V., J. C. Kitchen, and J. L. Müeller, 1993: Vertical structure of productivity and its vertical integration as derived from remotely sensed observations. *Limnol. Oceanogr.*, **38**, 1384–1393.

——, and R. W. Spinrad, 1980: An arctangent model of irradiance in the sea. *J. Geophys. Res.*, **85**, 4919–4922.

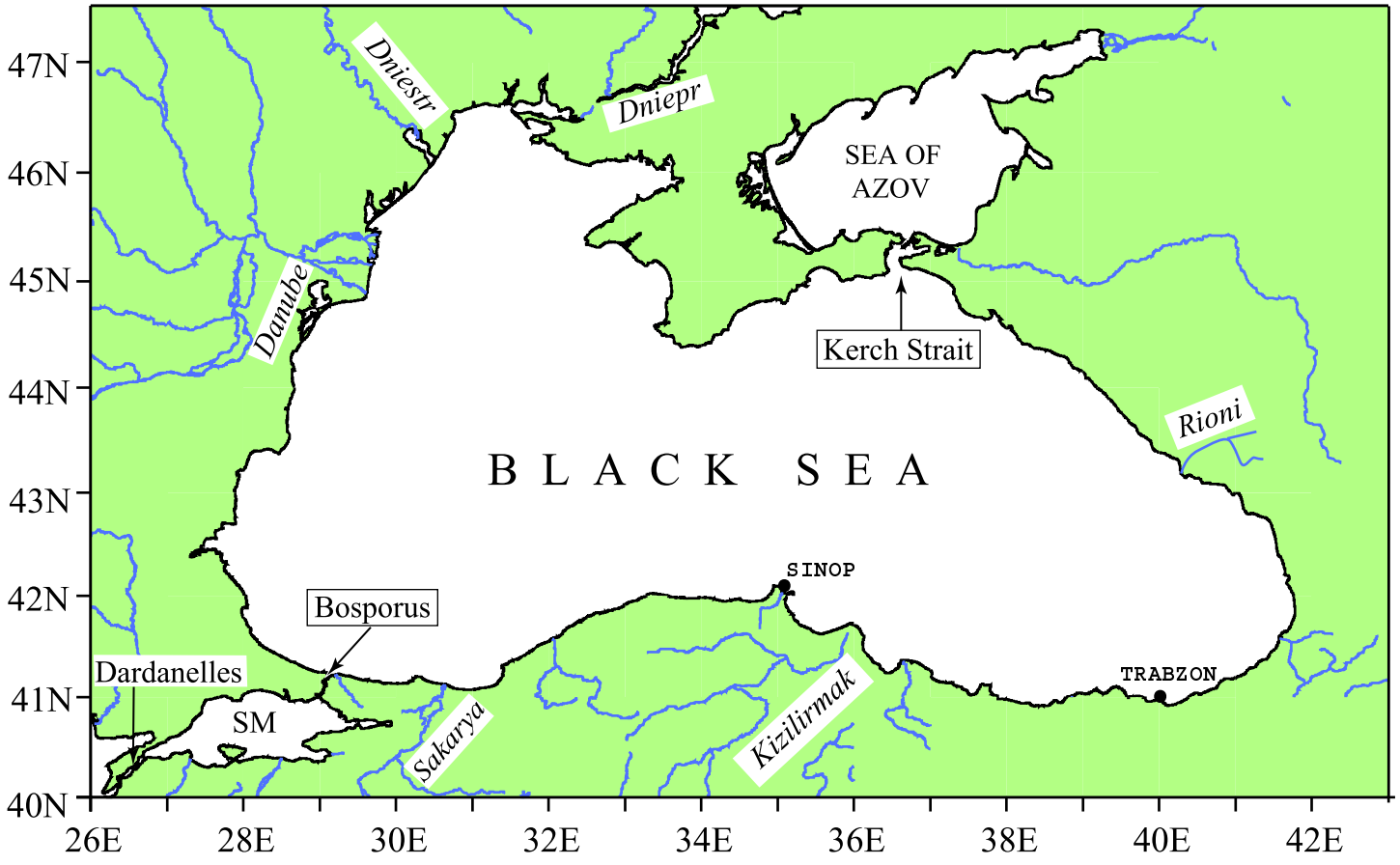

Figure 1: The geography of the Black Sea. Also shown are rivers discharged into the Black Sea. Only major rivers named on the map are used in the model simulations. The narrowest and widest points in the Sea of Marmara (SM) are 1.2 km and 6.4 km, respectively, and depth varies from 50 to 91 m in the main channel. Bosporus is $\approx$ 31 km long, with an average width of 1.5 km. It is only 0.7 km at its narrowest point with a sill depth of 30 m. The length of the Dardanelles is about 70 km with a general width ranging from 1.2 km to 2 km. Two coastal cities (Trabzon and Sinop) used in the text are also shown.

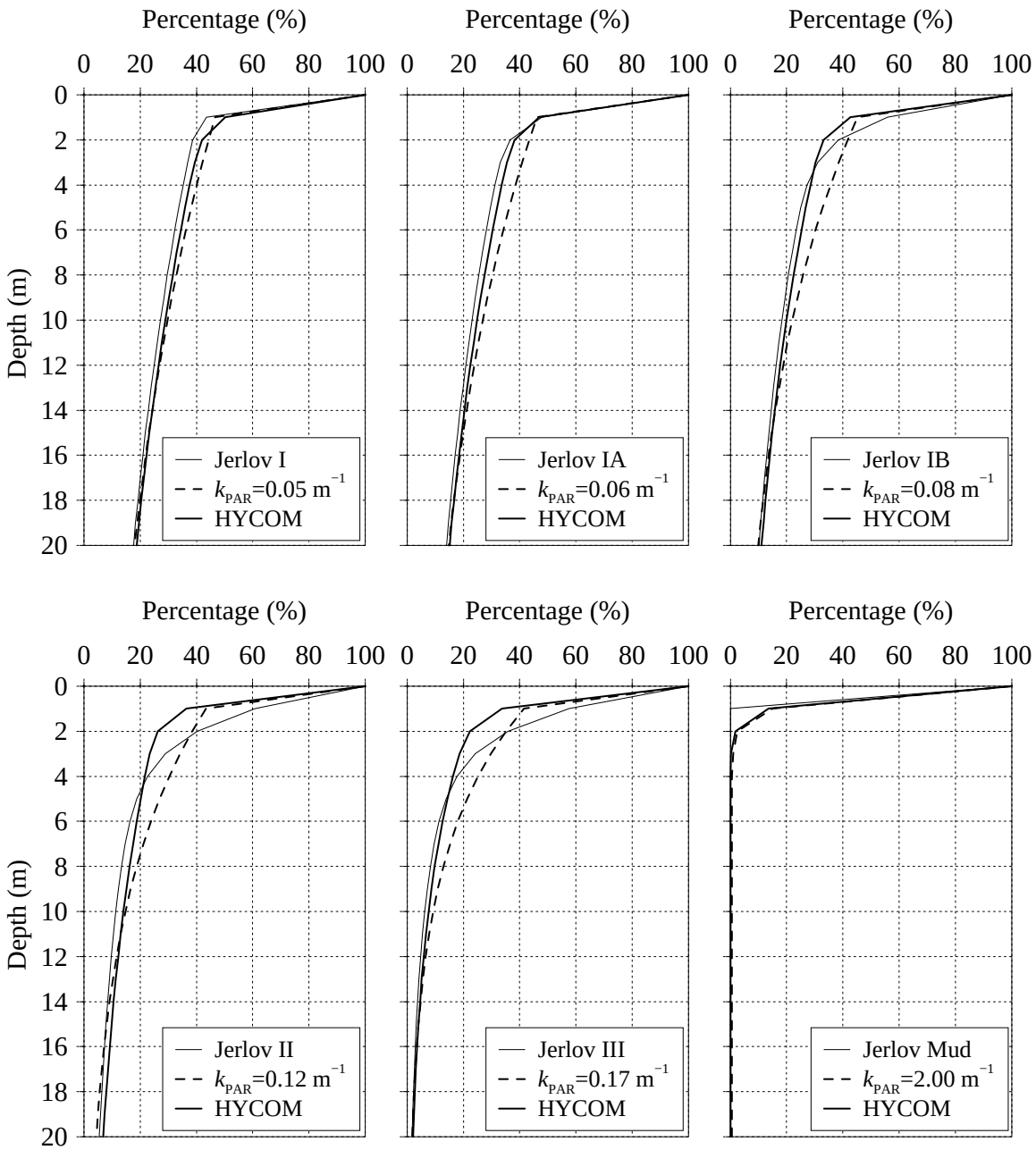

Figure 2: Percentage of shortwave radiation remaining below sea surface as a function of depth. The k_{PAR} values used in HYCOM are compared to the ones obtained from the tradiational Jerlov approach (Jerlov I, IA, IB, II, III and mud) and the ones used in a coarse vertical resolution OGCM, NLOM, (k_{PAR}=0.05, 0.06, 0.08, 0.12, 0.17 m^1 and mud). The HYCOM k_{PAR} values of 0.04345, 0.0500, 0.0588, 0.0714, 0.1266 and 2.00 m^1 correspond to Jerlov I, IA, IB, II, III and mud cases, respectively. Note that HYCOM uses a 0.5 m e–folding depth for the red spectrum so as k_{PAR} approaches 2.0, it matters little what fraction is in the each band because both bands have small 0.5 m e–folding depth.

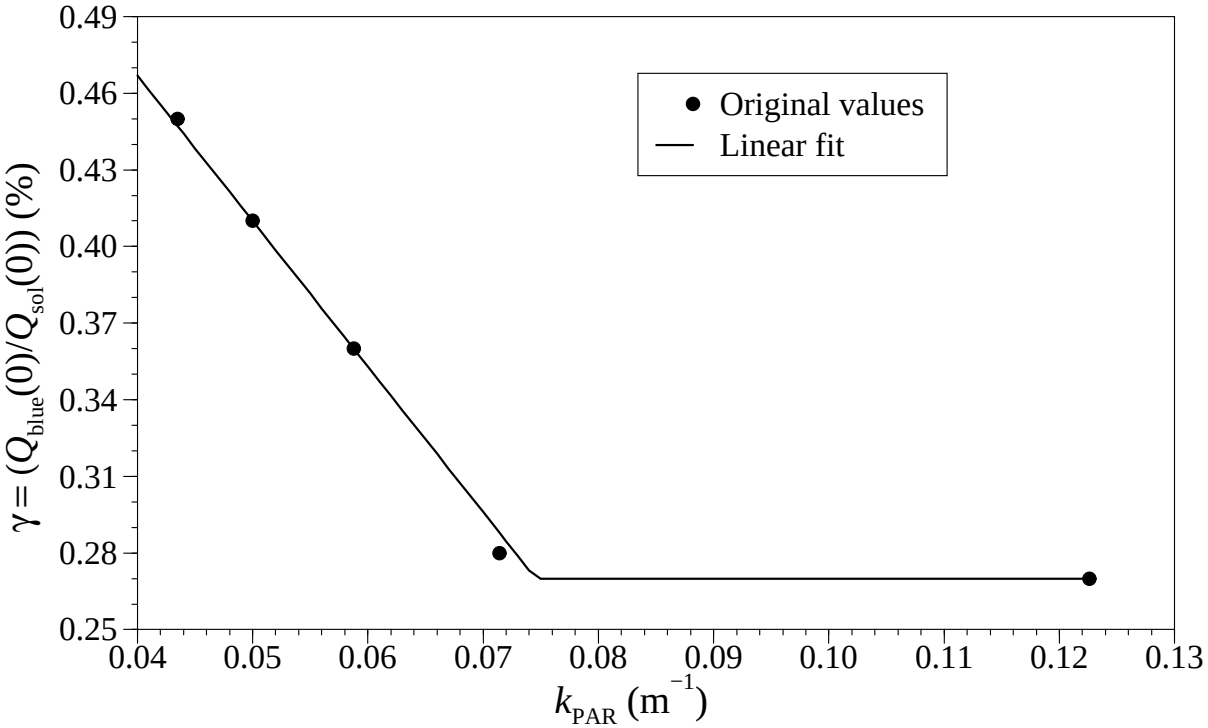

Figure 3: Percentage changes of $\gamma = Q_{\text{blue}}(0)/Q_{\text{sol}}(0)$ with k_{PAR}. Note that all PAR is assumed to represent primarily the blue spectrum.

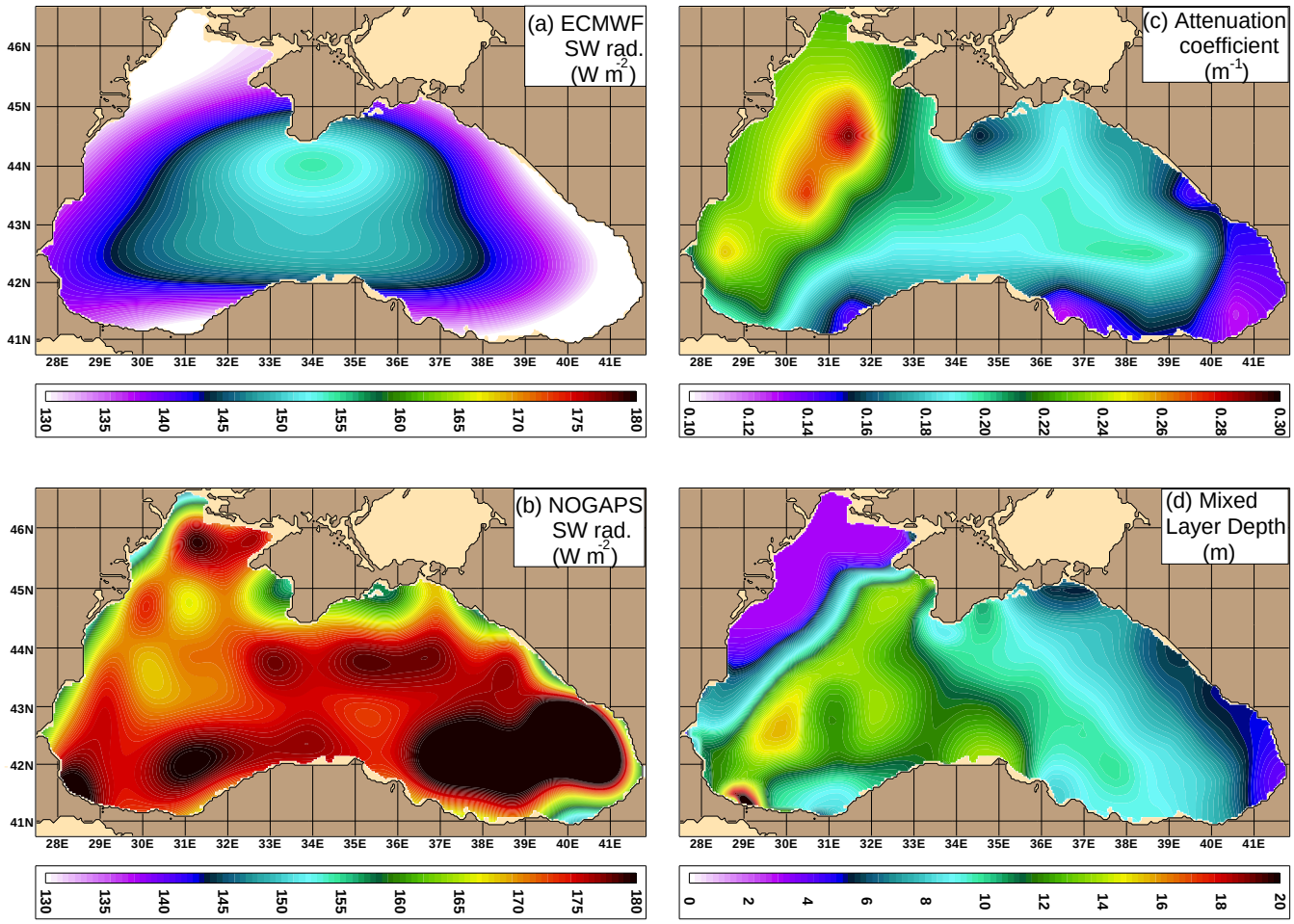

Figure 4: Climatological annual mean of various quantities over the Black Sea: (a) shortwave radiation at the sea surface (W m^{-2}) constructed from the 1.125° × 1.125° ECMWF re–analysis product (1979–1993), (b) shortwave radiation at the sea surface (W m^{-2}) constructed from the 1° × 1° NOGAPS product (1998–2002), (c) attenuation of Photosynthetically Available Radiation (m^{-1}) processed from the 1/12° SeaWiFS k_{490} data (1997–2001) as explained in the text, in detail, and (d) ocean mixed layer depth (m) based on the layer definition of Kara et al. (2000). The mixed layer depth (MLD) is defined as the depth at the base of an isopycnal layer, where the density has changed by a fixed amount of $\Delta\sigma_t = \sigma_t(T + \Delta T, S, P) - \sigma_t(T, S, P)$ from the density at a reference depth of 1 m. In this representation of MLD, S is the salinity, T is the temperature and P is pressure which is set to zero. Both ECMWF and NOGAPS provides relatively high frequency atmospheric forcing. Note that the color bars for (a) and (b) are same.

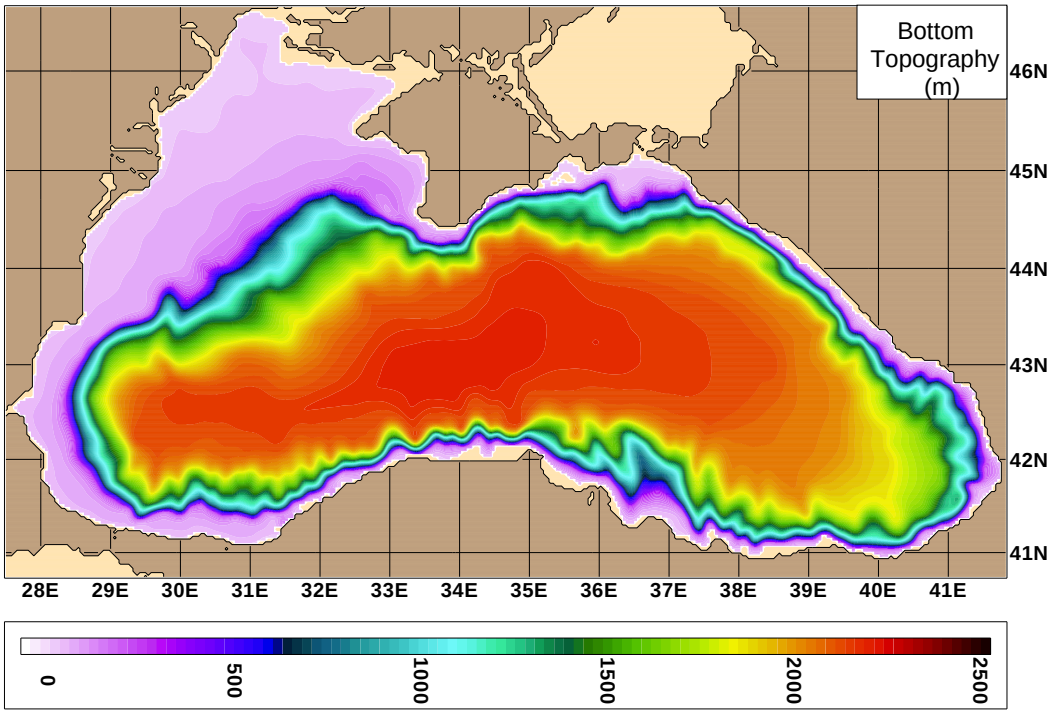

Figure 5: The bottom topography (m) and the model coastline used in HYCOM simulations. Note that the bottom topography includes 1–minute DBDB–V data. The model land-sea boundary is the 10–m isobath which is shown with light brown in color. The Sea of Azov is excluded in the model simulations. The DBDB–V data set was developed by NAVOCEANO to support the generation of bathymetric chart products. It provides bathymetric data to be integrated with other geophysical and environmental parameters for ocean modeling. The digitally rendered contours are put through a gridding routine. This routine takes the values that fall within a grid node area of influence, utilizing a multi–stage minimum–curvature spline algorithm. It should be noted that the abyssal plain of the Black Sea is ≈ 2000 m deep, and the maximum depth is ≈ 2204 m. The basin does not include large gulfs or islands but one of the most interesting features is the narrow continental shelf.

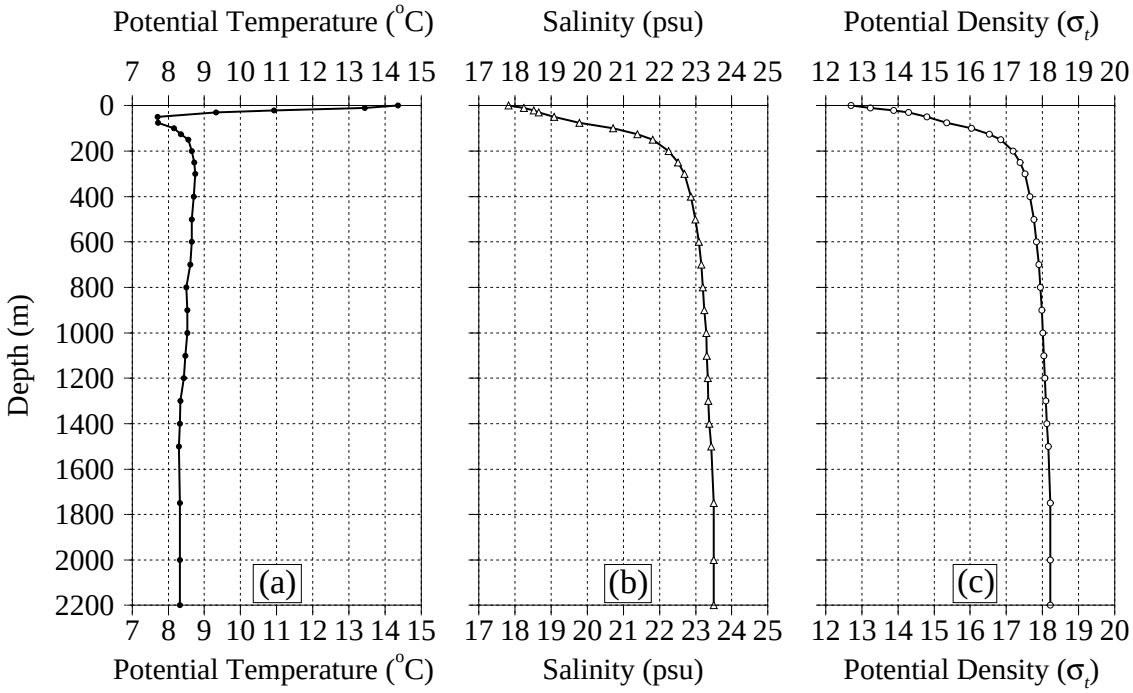

Figure 6: Annual mean of basin averaged potential temperature, salinity and potential density profiles obtained from the MODAS climatology. Standard depth levels in the climatology are 0, 10, 20, 30, 50, 75, 100, 125, 150, 200, 250, 300, 400, 500, 600, 700, 800, 900, 1000, 1100, 1200, 1300, 1400, 1500, 1750, 2000, 2200 m. The MODAS climatology does not include temperature/salinity below 1750 m in the Black Sea because the climatology is relaxed to the World Ocean Atlas 1994 at deeper layers, which is void of data in this region. In this case, a simple linear extrapolation was applied to the temperature and salinity data, and then the profiles were extended down to $\approx$ 2200 m. This linear interpolation is reasonable given the fact that temperature and salinity of the deep water masses do not change very much on the climatological time scales so they can be considered as quasi–steady.

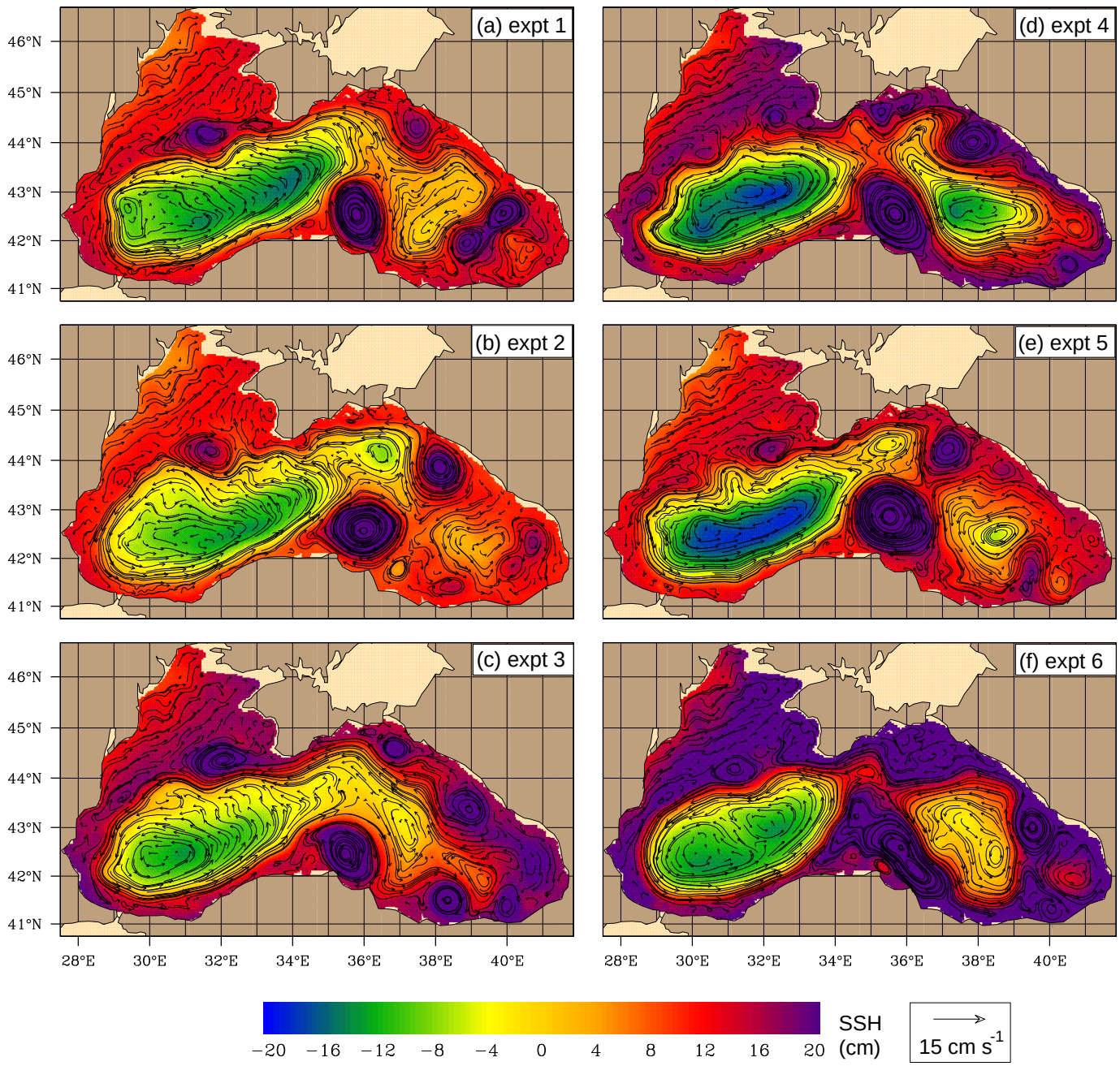

Figure 7: Snapshots of sea surface currents (cm s^{-1}) overlain on sea surface height (cm) in the Black Sea on March 2: Left panels from top to bottom, (a), (b) and (c), are for expts 1, 2 and 3 when HYCOM was forced with ECMWF wind and thermal fluxes. Similarly, right panels from top to bottom, (d), (e) and (f), are for expts 4, 5 and 6 when HYCOM was forced with NOGAPS wind and thermal fluxes. Note that the length of the reference velocity vector is 15 cm s^{-1}. See section 4d in the text for construction of the wind and thermal forcing fields.

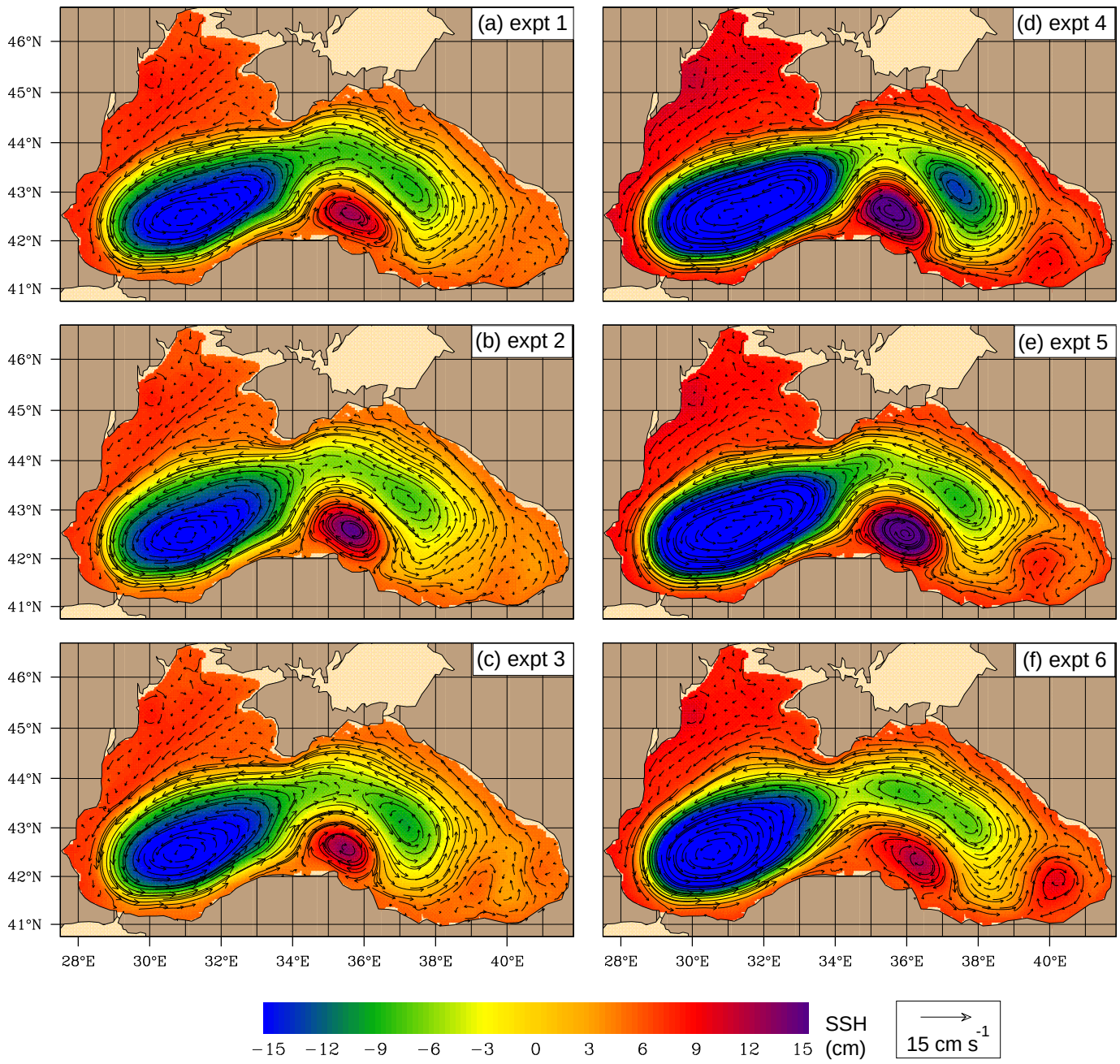

Figure 8: The annual mean sea surface currents (cm s^{-1}) overlain on annual mean sea surface heights (cm) in the Black Sea: Left panels from top to bottom, (a), (b) and (c), are for expts 1, 2 and 3 when HYCOM was forced with ECMWF wind and thermal fluxes. Similarly, right panels from top to bottom, (d), (e) and (f), are for expts 4, 5 and 6 when HYCOM was forced with NOGAPS wind and thermal fluxes. Note that the length of the reference velocity vector is 15 cm s^{-1}. The annual mean was formed using model years 5 through 8. Each field has basin wide mean SSH anomaly of zero.

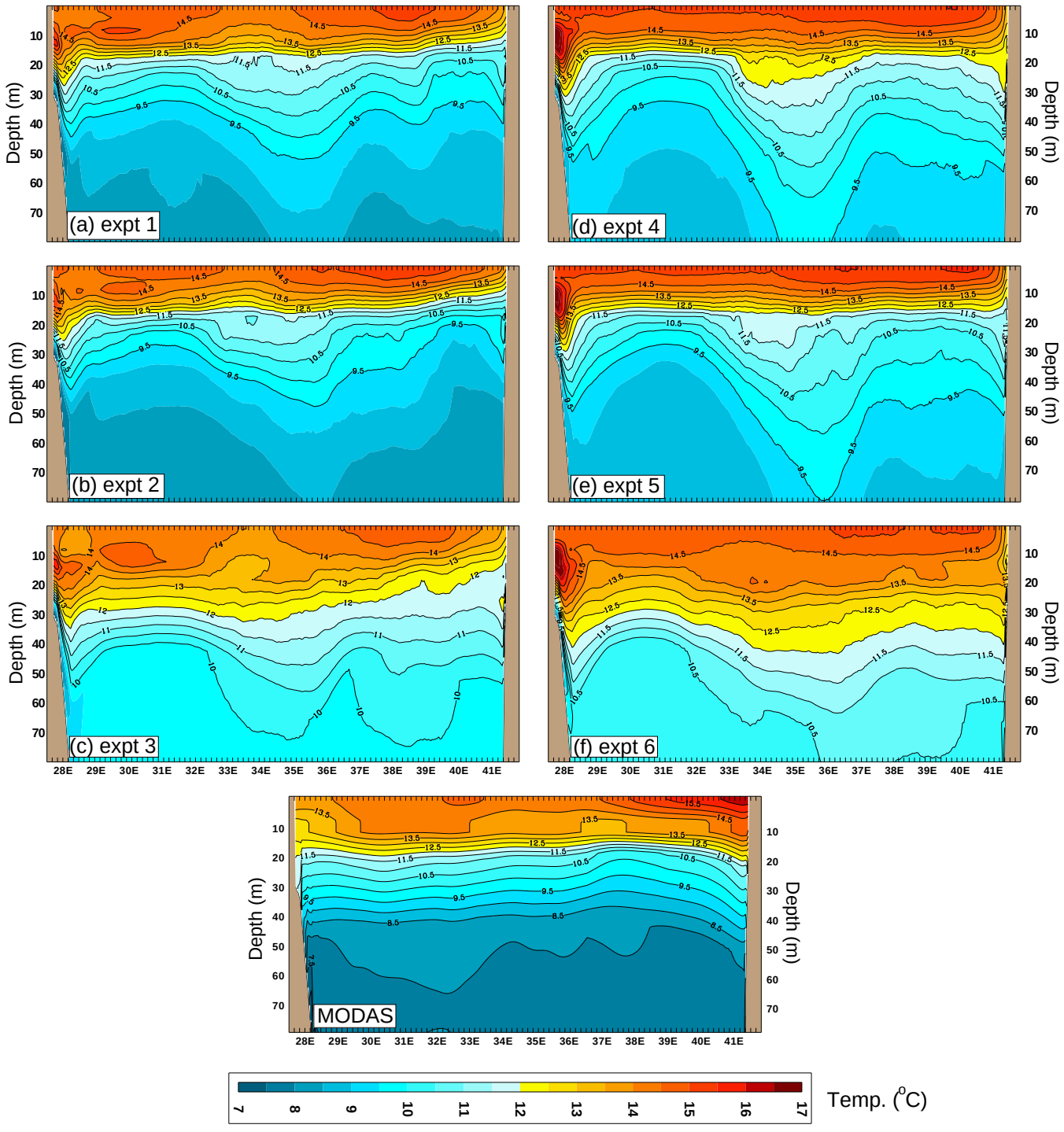

Figure 9: Black Sea annual mean cross–section of temperature along 42.62°N from the surface to 80 m depth. Results from expts 1 through 6 are shown in panels (a) through (f), respectively. The annual mean cross–section of MODAS temperatures is also shown for model–data comparison purposes. The climatological annual mean was formed using model years 5 through 8.

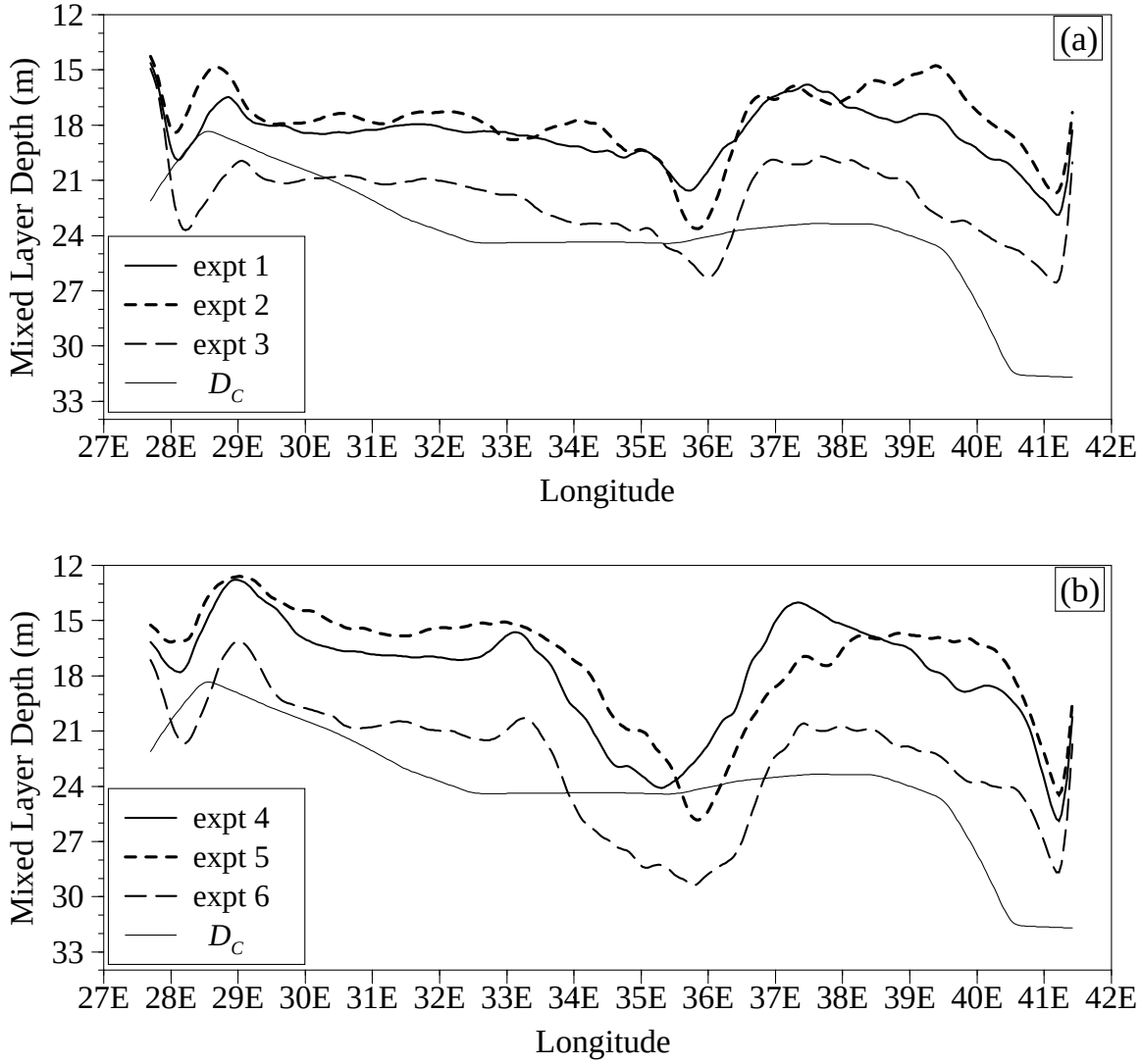

Figure 10: The annual mean MLD calculated along 42.62°N latitude in the Black Sea: (a) expts 1, 2 and 3 when the HYCOM was run with ECMWF wind/thermal forcing, and (b) expts 4, 5 and 6 when the HYCOM was run with NOGAPS wind/thermal forcing. The annual mean compensation depth, as defined in the text, is $D_C = \ln(0.01)/k_{\mathrm{PAR}}$.

Table 1: Percentage of shortwave radiation remaining under the Jerlov extinction. The percentage values are given for each Jerlov class.

Depth (m)	Jerlov I	Jerlov IA	Jerlov IB	Jerlov II	Jerlov III
0	100.00	100.00	100.00	100.00	100.00
1	43.54	47.86	55.76	60.95	57.57
2	38.69	36.60	38.40	40.24	35.77
3	36.87	33.12	31.00	28.98	24.20
4	35.30	31.19	27.31	22.63	17.74
5	33.79	29.61	25.04	18.84	13.88
6	32.36	28.15	23.35	16.39	11.37
7	30.98	26.78	21.92	14.67	9.60
8	29.66	25.47	20.64	13.36	8.25
9	28.40	24.23	19.44	12.28	7.17
10	27.19	23.05	18.33	11.26	6.20
11	26.03	21.92	17.28	10.48	5.47
12	24.93	20.85	16.29	9.76	4.82
13	23.87	19.84	15.36	9.09	4.24
14	22.85	18.87	14.48	8.46	3.74
15	21.88	17.95	13.66	7.88	3.29
20	17.60	13.98	10.18	5.51	1.75
30	11.40	8.48	5.65	2.70	0.49
40	7.38	5.14	3.14	1.32	0.14
50	4.78	3.12	1.74	0.65	0.04
60	3.09	1.89	0.97	0.32	0.01
70	2.00	1.15	0.54	0.15	0.00
80	1.30	0.70	0.30	0.08	0.00
90	0.84	0.42	0.17	0.04	0.00
100	0.54	0.26	0.09	0.02	0.00

Table 2: Percentage of shortwave radiation remaining under the HYCOM k_{PAR} extinction based on $\gamma = Q_{\mathrm{blue}}(0)/Q_{\mathrm{sol}}(0))$ values. The percentage values are given for k_{PAR} values of 0.0400, 0.0435, 0.0500, 0.0588, 0.0714, 0.1266, 0.2000, 0.5000, and 2.0000 m^{-1}.

γ (%)	0.4670	0.4472	0.4100	0.3597	0.2879	0.2700	0.2700	0.2700	0.2700
Depth (m)	0.0400	0.0435	0.0500	0.0588	0.0714	0.1266	0.2000	0.5000	2.0000
0	100.00	100.00	100.00	100.00	100.00	100.00	100.00	100.00	100.00
1	52.08	50.30	46.99	42.58	36.44	33.67	31.99	26.26	13.53
2	44.09	42.01	38.18	33.15	26.26	22.30	19.44	11.27	1.83
3	41.55	39.39	35.44	30.31	23.41	18.65	15.00	6.21	0.25
4	39.81	37.60	33.59	28.45	21.66	16.30	12.16	3.68	0.03
5	38.24	35.98	31.93	26.81	20.14	14.34	9.94	2.22	0.00
6	36.74	34.45	30.37	25.27	18.75	12.63	8.13	1.34	0.00
7	35.30	32.98	28.89	23.83	17.46	11.13	6.66	0.82	0.00
8	33.91	31.58	27.48	22.47	16.26	9.81	5.45	0.49	0.00
9	32.58	30.24	26.14	21.18	15.14	8.64	4.46	0.30	0.00
10	31.30	28.95	24.87	19.97	14.09	7.61	3.65	0.18	0.00
11	30.08	27.72	23.65	18.83	13.12	6.71	2.99	0.11	0.00
12	28.90	26.54	22.50	17.76	12.22	5.91	2.45	0.07	0.00
13	27.76	25.41	21.40	16.74	11.37	5.21	2.01	0.04	0.00
14	26.68	24.33	20.36	15.79	10.59	4.59	1.64	0.02	0.00
15	25.63	23.29	19.37	14.88	9.86	4.04	1.34	0.01	0.00
20	20.98	18.74	15.08	11.09	6.90	2.15	0.49	0.00	0.00
30	14.07	12.13	9.15	6.16	3.38	0.61	0.07	0.00	0.00
40	9.43	7.86	5.55	3.42	1.65	0.17	0.01	0.00	0.00
50	6.32	5.09	3.37	1.90	0.81	0.05	0.00	0.00	0.00
60	4.24	3.29	2.04	1.05	0.40	0.01	0.00	0.00	0.00
70	2.84	2.13	1.24	0.59	0.19	0.00	0.00	0.00	0.00
80	1.90	1.38	0.75	0.33	0.09	0.00	0.00	0.00	0.00
90	1.28	0.89	0.46	0.18	0.05	0.00	0.00	0.00	0.00
100	0.86	0.58	0.28	0.10	0.02	0.00	0.00	0.00	0.00

Table 3: Constant parameters used in the HYCOM Black Sea model based on a series of tuning experiments.

Value	Description of the constant used in the Black Sea Model
0.1	deformation–dependent Laplacian viscosity factor
5.e-3	diffusion velocity for Laplacian momentum dissipation (m s^{-1})
67.e-4	diffusion velocity for biharmonic momentum dissipation (m s^{-1})
0.05	diffusion velocity for biharmonic thickness diffusion (m s^{-1})
5.e-2	diffusion velocity for Laplacian temp/saln diffusion (m s^{-1})
2.e-3	coefficient of quadratic bottom friction
10.0	thickness of bottom boundary layer (m)
0.02	minimum density jump across interfaces (kg m^{-3})
0.2	equivalent temperature jump across mixed–layer (°C)
30.0	reference mixed–layer thickness for SSS relaxation (m)
0.3	KPP critical bulk richardson number
0.7	KPP value for calculating rshear instability
50.e-4	KPP max viscosity and diffusivity due to shear instability (m^2 s^{-1})
1.e-4	KPP: background/internal wave viscosity (m^2 s^{-1})
1.e-5	KPP background/internal wave diffusivity (m^2 s^{-1})
10.e-4	KPP salt fingering diffusivity factor (m^2 s^{-1})
1.9	KPP salt fingering factor
98.96	KPP value for nonlocal flux term
10.0	KPP value for nonlocal flux adjustment term
1.8	KPP value for turbulent shear contributon to bulk Ri number
5.0	KPP value for turbulent velocity scale

Table 4: Annual mean flow values obtained from four climatological data sets for the rivers discharged into the Black Sea. The source for the Perry data is Perry et al. (1996), RivDIS (http://daac.ornl.gov/rivdis/) and UCAR (http://dss.ucar.edu/datasets/ds552.1/). Final data product was constructed in the NRL using the Perry data set. The NRL data set is similar to RivDIS except a scale factor that is obtained from Perry et al. (1996) to correct the annual mean. The Perry data set is a compilation of data from many sources and had one mean value for each river. Note that 1 Sv $= 10^6$ m^3 s^{-1} $\approx$ 32000 km^3 y^{-1}. There are also other rivers which are not listed in the table, such as the Southern Bug (Ukranie) and Kamtehiya (Bulgaria), discharged into the Black Sea; however, they are not input to the model because the contribution from these rivers are very small. The Bosporus is considered as a negative precipitation point to balance the evaporation minus precipitation field over the Black Sea.

River	Perry ($m^3\ s^{-1}$)	RivDIS ($m^3\ s^{-1}$)	UCAR ($m^3\ s^{-1}$)	NRL ($m^3\ s^{-1}$)
Danube	6365.0	6499.0	6413.6	6114.1
Dniepr	1630.8	1482.2	1483.7	1630.0
Rioni	409.7	408.6	402.7	409.7
Dniestr	326.3	375.2	324.3	326.3
Sakarya	217.3	192.3	192.8	217.6
Kizilirmak	180.5	201.8	202.2	202.2
River	Perry ($km^3\ y^{-1}$)	RivDIS ($km^3\ y^{-1}$)	UCAR ($km^3\ y^{-1}$)	NRL ($km^3\ y^{-1}$)
Danube	203.7	205.0	205.2	195.7
Dniepr	52.2	46.7	47.5	52.2
Rioni	13.1	12.9	12.9	13.1
Dniestr	10.4	11.8	10.4	10.4
Sakarya	7.0	6.1	6.2	7.0
Kizilirmak	5.8	6.4	6.5	6.5

Table 5: Time periods during which climatological river discharges were constructed. Total number of years for the climatology is also included. Note that the Perry data set was constructed using annual mean for individual years so the total number of years represents total of these individual years. The other two data sets were constructed using monthly mean discharge values.

River	Perry		RivDIS		UCAR	
	Climatology	Year	Climatology	Year	Climatology	Year
Danube	1962–1994	14	1921–1984	64	1921–2000	80
Dniepr	1962–1994	10	1952–1984	33	1952–1984	33
Rioni	1975–1994	3	1965–1984	20	1928–1984	57
Dniestr	1975–1991	4	1965–1984	20	1881–1985	76
Sakarya	1975–1991	3	1976–1983	8	1976–1983	8
Kizilirmak	1975–1991	2	1976–1983	8	1976–1983	8

Table 6: Six HYCOM simulations used in this paper. The simulations were performed using several massively parallel supercomputers. The model array size is 360×206, and performing a 1–month simulation takes ≈ 2.3 wall–clock hours using 64 IBM SP POWER3 processors or ≈ 0.7 wall–clock hours using 64 HP/COMPACT SC45 processors. A linear regression analysis was performed for domain averaged parameters (layer temperature, salinity, potential and kinetic energy, etc.) to investigate statistical equilibrium in each layer, and is expressed numerically as % change per decade. The model is deemed to be in statistical equilibrium when the rate of potential energy change is acceptably small (e.g., $< 1\%$ in 5 years) in all layers. Note that the model uses climatological wind and thermal forcing (i.e., air temperature at 10 m, air mixing ratio at 10 m, shortwave and longwave radiation) constructed from ECMWF Re–Analysis (ERA) or NOGAPS as explained in text, in detail.

Expt.	k_{PAR}	Description of the experiment	Forcing
expt 1	Variable	Spatial and temporal attenuation depths	ECMWF
expt 2	99 m^{-1}	All solar radiation absorbed at the surface	ECMWF
expt 3	0.06 m^{-1}	Constant attenuation depth in the Black Sea	ECMWF
expt 4	Variable	Spatial and temporal attenuation depths	NOGAPS
expt 5	99 m^{-1}	All solar radiation absorbed at the surface	NOGAPS
expt 6	0.06 m^{-1}	Constant attenuation depth in the Black Sea	NOGAPS